Louisiana State University

LSU Digital Commons

1973

Energy Bands in Paramagnetic Chromium.

Jagannath Rath
Louisiana State University and Agricultural & Mechanical College

Follow this and additional works at: https://digitalcommons.lsu.edu/gradschool_disstheses

INFORMATION TO USERS

This material was produced from a microfilm copy of the original document. While the most advanced technological means to photograph and reproduce this document have been used, the quality is heavily dependent upon the quality of the original submitted.

The following explanation of techniques is provided to help you understand markings or patterns which may appear on this reproduction.

1. The sign or "target" for pages apparently lacking from the document photographed is "Missing Page(s)". If it was possible to obtain the missing page(s) or section, they are spliced into the film along with adjacent pages. This may have necessitated cutting thru an image and duplicating adjacent pages to insure you complete continuity.

2. When an image on the film is obliterated with a large round black mark, it is an indication that the photographer suspected that the copy may have moved during exposure and thus cause a blurred image. You will find a good image of the page in the adjacent frame.

3. When a map, drawing or chart, etc., was part of the material being photographed the photographer followed a definite method in "sectioning" the material. It is customary to begin photoing at the upper left hand corner of a large sheet and to continue photoing from left to right in equal sections with a small overlap. If necessary, sectioning is continued again — beginning below the first row and continuing on until complete.

4. The majority of users indicate that the textual content is of greatest value, however, a somewhat higher quality reproduction could be made from "photographs" if essential to the understanding of the dissertation. Silver prints of "photographs" may be ordered at additional charge by writing the Order Department, giving the catalog number, title, author and specific pages you wish reproduced.

5. PLEASE NOTE: Some pages may have indistinct print. Filmed as received.

74-7254

RATH, Jagannath, 1946-
  ENERGY BANDS IN PARAMAGNETIC CHROMIUM.

  The Louisiana State University and
  Agricultural and Mechanical College,
  Ph.D., 1973
  Physics, solid state

University Microfilms, A XEROX Company, Ann Arbor, Michigan

Energy Bands in Paramagnetic Chromium

A Dissertation

Submitted to the Graduate Faculty of the
Louisiana State University and
Agricultural and Mechanical College
in partial fulfillment of the
requirements for the degree of
Doctor of Philosophy

in

The Department of Physics and Astronomy

by

Jagannath Rath
M.S., University of Illinois, Chicago, 1969
August, 1973

ACKNOWLEDGEMENT

TABLE OF CONTENTS

LIST OF TABLES

LIST OF FIGURES

ABSTRACT

The results of a self-consistent tight binding calculation of the band structure of paramagnetic chromium are reported. The basis set consisted of atomic wave functions for the 1s, 2s, 3s, 4s, 2p, 3p, and 4p states expressed as linear combinations of Gaussian-type orbitals (GTO) and five individual GTO for each 3d state. The exchange potential was calculated according to the $X\alpha$ method with $\alpha=2/3$. The initial Coulomb potential was constructed from the superposed charge densities of neutral chromium atoms in a $3d^5 4s^1$ configuration. Eleven iterations were required to determine a self-consistent potential. The charge density was sampled at 55 inequivalent points in 1/48th of the zone. The density of states was calculated according to the Gilat-Raubenheimer method. Cross sections of the Fermi surface were obtained in several symmetry planes. The X-ray form factor was determined from the self-consistent wave functions. The Compton profile in various directions was also calculated using the above wave functions.

CHAPTER I: INTRODUCTION

The calculation of energy bands and wave functions for the transition metals is a central problem in solid state physics. These quantites are of importance in the construction of a band theory of itinerant electron magnetism. Energy band calculations have reproduced the observed shape of the Fermi surface in molybdenum and tungsten[1] even though the effects of electron correlations in transition metals may be significant for other problems. Recent band structure studies for iron and nickel[2,3] have been equally successful. They reproduce the shape of the experimentally observed Fermi surface fairly well and give a reasonable value for the magnetic moment. In the present work, we shall discuss a band structure calculation for paramagnetic chromium. We have applied the tight binding method to compute the energy bands and wave functions of this metal. Chromium presents a particularly interesting problem for band theory because it exhibits itinerant antiferromagnetism. The structure of the Fermi surface of nonmagnetic chromium can be related to the specific magnetic structure of the low temperature, antiferromagnetic phase. We shall discuss this in some detail.

Below the temperature $T_N=312^{\circ}K$, pure chromium is an antiferromagnet. Neutron diffraction studies have

1

indicated that the antiferromagnetism in chromium can not
be described by the usual two sublattice model of anti-
ferromagnetism. The spin distribution in chromium has a
periodic sinusoidal modulation in the [100] directions.
The wave vector of this sinusoidal modulation is in-
commensurate with the lattice periodicity and is dependent
on the temperature and the impurity concentration. At the
maximum of this sinusoidal distribution, the moment per
atom is about 0.59 μ_B. Above $120^{\circ}K$, the sinusoidal wave
is transverse and below, it is longitudinal. This spin
structure is described by a spin density wave (SDW). A
SDW is a self-consistent field solution for the interacting
electrons which exhibits spatially periodic magnetization.

Overhauser[4,5] pointed out that the ground state of an
interacting electron gas with unscreened Coulomb inter-
action in the Hartree-Fock approximation is described by
a SDW. However, subsequent analysis of Rajagopal,[6] Fedders
and Martin[7] and Hamann and Overhauser[8] has indicated that
if the interaction is screened, so that it has the form
$e^{-\xi r}/r$, there exists a certain reciprocal screening length
(ξ_{max}) such that if $\xi < \xi_{max}$, the SDW state is lower in
energy than the paramagnetic state while if $\xi > \xi_{max}$, there
is no SDW state at all. If ξ has the Thomas-Fermi value,
the system remains in the paramagnetic state.

It was first pointed out by Lomer[9] that in real
solids, particular features of the Fermi surface can

produce SDW antiferromagnetism. Lomer proposed a Fermi surface for nonmagnetic chromium based on Wood's band calculation for nonmagnetic iron. This consisted of closed electron and hole surfaces around Γ and H, respectively, hole pockets around N, and electron balls along the 100 axis. A model of the chromium Fermi surface similar to that of Lomer was also derived by Matheiss[49] from an APW band calculation for tungsten. The essential physical concept of Lomer's model is that "nesting" among portions of the Fermi surface leads to the SDW state. It is assumed that a portion of the electron Fermi surface centered around Γ is quite similar to the hole Fermi surface centered at the zone corner H. Corresponding points on these two pieces of the Fermi surface can be connected by a vector $\underset{\sim}{Q}$, such that $\underset{\sim}{Q}$ is nearly constant. This property is called "nesting."

The linear response of interacting electrons in a crystal lattice to a magnetic field with vector $\vec{q}$ is described by a susceptibility function $\chi(\vec{q},\vec{q}+\vec{K})$, where $\vec{K}$ is a reciprocal lattice vector. A divergence in this susceptibility function for some value of $\vec{q}$ indicates a magnetic instability of the system. If the divergence occurs at $\vec{q}\neq0$ the paramagnetic state is unstable towards a magnetic state which exhibits a periodic magnetization with wave vector $\vec{q}$. This new magnetic state can be described by a SDW.

There is, unfortunately, no way to calculate $\chi(\vec{q},\vec{q}+\vec{K})$ exactly. Some information about this susceptibility function can be obtained from a calculation of the analogous susceptibility function for noninteracting electrons, $\chi^O(\vec{q},\vec{q}+\vec{K})$. For many purposes an average susceptibility function $\bar{\chi}^O(\vec{q})$ can be used, which properly weighs the $\chi^O(\vec{q},\vec{q}+\vec{K})$ for various $\vec{K}$, and so eliminates the latter variable. Then if the effective interaction (I) is short-ranged, the random phase approximation yields the expression for the interacting electron susceptibility function as, $\bar{\chi}(q) = \bar{\chi}^O(\vec{q})/(1-I\ \bar{\chi}^O(\vec{q}))$. Instabilities would occur when $I\ \bar{\chi}^O(\vec{q}) > 1$, and a maximum in $\bar{\chi}^O(\vec{q})$ (or more generally in $\chi^O(\vec{q},\vec{q}+\vec{K})$) will indicate a periodicity at which the paramagnetic system may be unstable.

The Fermi surface of nonmagnetic chromium strongly suggests the possiblity of a SDW instability. This results from the "nesting" property mentioned earlier. The "nesting" of portions of the Fermi surface would lead to small energy dominators in the expression for $\chi^O(\vec{q},\vec{q}+\vec{K})$. Thus at $\vec{q}=\vec{Q}$, one would expect a maxima for this function. Calculations of generalized susceptibility function $\chi(\vec{q},\vec{q}+\vec{K})$ have been reported in the literature.[10] We shall discuss the results of one such calculation.

There have been several calculations[11] which have employed simple models to discuss SDW antiferromagnetism

in chromium and its alloys. The emphasis of this work will, however, be placed on a detailed study of the energy bands of real chromium in the paramagnetic phase. We will first review some aspects of previous band calculations for this material.

The vast majority of energy band calculations that have been made for transition metals and their compounds have employed the Augmented Plane Wave (APW) method and the Green's function (KKR) method. In their usual forms these methods assume that the potential is spherically symmetric within a sphere inscribed in an atomic cell, and is constant outside (the muffin-tin potential). This appears to be a reasonable approximation in the case of metals whose band structure is free electron like. In the case of transition metals where d electrons are particularly sensitive to the nonspherical part of the potential (the crystal field effects) the choice of a muffin-tin potential may not be suitable.

The first reported band calculation for nonmagnetic chromium was performed by Asdente and Friedel[12] using the tight binding method. The interaction of the 3d band with 4s-4p bands and all the three center integrals and overlap integrals occurring in this calculation were neglected. These approximations were so severe that quantitative results could not be obtained.

Loucks[13] used the APW method to study energy bands in nonmagnetic chromium. A Coulomb potential was generated by a superposition of atomic potentials which were obtained from Hartree-Fock Slater self-consistent calculations similar to those of Herman and Skillman. The exchange potential was constructed using the $X\alpha$ method, and the full value of exchange coefficient, $\alpha=1$, was used. We shall discuss the construction of the exchange potential and the $X\alpha$ method in Chapter II. The Fermi surface obtained was in rough agreement with Lomer's model except that the hole pockets around N were absent. The existence of these hole pockets in antiferromagnetic chromium has been established from de Haas-van Alphen studies.[15] The magnitude of the nesting wave vector $\vec{Q}$ was not reported in this work.

Switendick[16] reported results for the charge and spin densities obtained for chromium from a self-consistent form of the APW method, but experienced difficulties in obtaining convergence to the proper antiferromagnetic state as the number of iterations was increased.

Asano and Yamashita[17] applied the KKR (Green's function) method in a calculation of the band structures of both the paramagnetic and antiferromagnetic phases of chromium. Their calculations were only approximately self-consistent. Exchange was included, as in the work of

Loucks ($X\alpha$, $\alpha=1$), and a somewhat ad hoc correlation was imposed in the spirit of Wigner-Seitz method. They obtained a Fermi surface for paramagnetic chromium that was consistent with Lomer's model. In the case of anti-ferromagnetic chromium, they considered a hypothetical state where the wave vector of the nesting vector $\underset{\sim}{Q}$ was given as $\frac{2\pi}{a}$ (.95,0,0). Although their procedure differs from ours, the resulting Fermi surface seems to be similar.

Additional band calculations for paramagnetic chromium have been reported by Yasui, Hayashi and Shimizu[18] and by Gupta and Sinha.[10] Yasui, et al. employed a combination of the tight binding and OPW methods for the band calculation. The calculation was carried to self-consistency for two values of the exchange paramater α in the $X\alpha$ method ($\alpha=1.0$ and $\alpha=.725$). The Fermi surface obtained for $\alpha=1$ led to an antiferromagnetic periodicity characterized by $\underset{\sim}{Q} = \frac{2\pi}{a}$ (1,0,0). However, for the exchange parameter $\alpha=.725$, the reported value of $\underset{\sim}{Q}$ was $\underset{\sim}{Q} = \frac{2\pi}{a}$ (.97,0,0).

In the course of a calculation of the wave vector dependent magnetic susceptibility of chromium, Gupta and Sinha[10] reported a computation of the band structure by the APW method. The exchange potential was constructed in the $X\alpha$ method with $\alpha=1$. The Coulomb potential was

constructed from the atomic charge densities obtained in the self-consistent field atomic calculation of Liberman, et al. This calculation was not iterated to self-consistency. The unenhanced generalized susceptibility without the inclusion of oscillator-strength matrix elements showed a peak at the nesting vector $Q = \frac{2\pi}{a}$ (.88,0,0). When the matrix elements were included to compute the above function there was a broad peak in addition to a peak at $Q = \frac{2\pi}{a}$ (.88,0,0). A calculation of the exchange enhanced generalized susceptibility function again showed a maximum at $Q = \frac{2\pi}{a}$ (.88,0,0).

The investigation described here used themodified tight binding method[19] to compute the energy bands and wave functions. This method has recently been applied to iron [20] and niciel.[21] The Coulomb part of the crystal potential for the first stage of the iterative process was constructed from a superposition of the charge densities for a system of neutral chromium atoms, each atom being in the $3d^5 4s^1$ configuration. The exchange potential was constructed in the Xα method with $\alpha=2/3$. The potential used in the present calculation was not of the muffin-tin type. The energy eigenvalues and eigenfunctions were calculated at 55 distinct points in 1/48th of the Brillouin Zone. The wave functions obtained were utilized to initiate a self-consistency procedure[22]

(described in Chapter II). After a self-consistent poten-
tial had been obtained, energy bands and wave functions
were calculated at 819 distinct points in 1/48th of the
Brillouin Zone. The density of states was constructed
using the Gilat-Raubenheimer[23] method. Contributions
from the critical points of the energy bands were included
in the density of states calculation. Cross sections of
the Fermi surface in various symmetry planes were obtained.
X-ray form factors were calculated using the self-consistent
wave functions. Compton profiles were also calculated.
In Chapter III we shall outline the theory of scattering
of X-rays from a system of electrons. Details of the
result are presented in Chapter IV.

This is a calculation of the energy bands and the
associated wave functions in the spirit of the one-
electron approximation. The choice of the exchange
parameter α is somewhat arbitrary. The results obtained
in the present calculation are in fair agreement with
those obtained using other methods. The present method
has the advantage that it is easy to obtain the energy
bands and wavefunctions at a large number of points in
the Brillouin Zone without resorting to an interpolation
scheme. The results obtained in this calculation will be
used subsequently to calculate the wave vector dependent
magnetic susceptibility.

In the next chapter we shall discuss the one-electron approximation, the modified tight binding method and the self-consistency procedure.

CHAPTER II: THE TIGHT BINDING METHOD
AND SELF-CONSISTENCY PROCEDURE

This chapter is divided into three sections. In Section I, we shall briefly discuss the one-electron approximation. In Section II, we shall discuss the choice of a basis set for the calculations, and the construction of a one-electron potential. In Section III, we shall outline the tight binding method and discuss the self-consistency procedure followed in the present calculation.

Section I. The One-Electron Approximation

The calculation of electronic eigenstates in crystals is essentially a many body problem and requires the solution of Schrödinger's equation for a very large number of nuclei and electrons. Thus to solve this problem one has to make numerous simplifying assumptions. The first approximation that enters into the consideration is the Born-Oppenheimer approximation in which one assumes that the motion of the electrons to be independent of the motion of the nuclei. Even after making the Born-Oppenheimer approximation one has to solve the Schrödinger equation for a system of interacting electrons embedded in a periodic lattice. The next approximation that is generally made is that each electron moves in an average periodic field of other electrons and nuclei. This

approximation reduces the many electron problem to a

simpler problem of an electron in a periodic potential and

is due to Hartree and Fock. In the Hartree approximation,

one neglects all electron-electron correlation and in the

Hartree-Fock approximation one includes only those

electron-electron correlations arising from the Pauli ex-

clusion principle. In the Hartree theory the exchange

effects are also absent. However, it must be stressed the

exchange and the correlation processes have important

effects and many attempts have been made to include these

effects in the independent electron model of the electronic

properties of the solids with some success. In materials

with narrow energy bands the electron-electron correla-

tions can lead to properties that could be attributed to

both localized and itinerant properties of the electrons.[24]

The intra-atomic exchange and correlation interactions lead

to local moment formation; they are also responsible for

spin wave like excitations in ferromagnetic metals, large

itinerant d-electron contribution to the specific heat,

fractional magnetic moments, and other properties charac-

teristic of itinerant electrons. Also, it is believed that

intra-atomic electron-electron correlations play an

important role in bringing about ferromagnetism in the

transition metals.[25]

It has been recognized that the effects of electron-

electron exchange and correlation effects must be taken

into account simultaneously. In the Hartree theory, even though the Pauli exclusion principle is not taken into account, certain properties of conduction electrons can be explained. When one includes the exchange interactions without considering any correlation effects, this agreement with experiments disappears, because the density of states vanishes at the Fermi energy. Raimes[26] has pointed out that by including correlations in Hartree-Fock theory some of the original agreement is restored. Slater pointed out that many of the difficulties in Hartree-Fock theory, especially those connected with the vanishing of the density of states at Fermi energy are due to the nonlocal nature of the exchange operator. He suggested a local average exchange potential[27] as a further approximation to avoid these difficulties. Such an approximation has come to be known as the $[\rho(r)]^{1/3}$ approximation. A large number of band structure calculations have been performed with this average exchange potential. Recently there have been some discussions as to the magnitude of the exchange potential. Here we shall briefly outline the derivation of the one electron Schrödinger equation for spin orbital $\psi_i(\vec{r})$ and discuss the exchange potential that enters into such an equation. This method has come to be known as $X\alpha$[28] method, where α stands for a certain multiplicative factor that appears in the average exchange potential. The one-electron Schrödinger equation is

derived by a variational principle; an expression for the total energy suggested in the work of Gaspar, Kohn, and Sham,[29] is used in setting up this variational principle.

The expression for the total energy involves the occupation number, n_i, of the spin orbitals. They are zero for the empty orbitals, unity for occupied orbitals. In certain cases fractional values of n_i may be needed. In terms of the occupation number, n_i, and spin orbitals $\psi_i(\vec{r}_1)$, one has the expression for the charge density

$$\rho(\vec{r}_1) = \sum_i n_i \, \psi_i^*(\vec{r}_1) \psi_i(\vec{r}_1) \qquad (2.1)$$

This sum includes both spin up and spin down orbitals. The Hamiltonian consists of a one-electron operator f_1 which includes (i) kinetic energy of the electrons, (ii) potential energy of the electrons in the field of nuclei, and a two-electron operator $g(\vec{r}_1,\vec{r}_2)$ corresponding to coulomb interaction between pairs of electrons. There is also an internuclear interaction term that must be included in calculation of the total energy. This will not be included here because we are interested only in single particle electronic energy. The total energy is expressed in the form

$$\langle E \rangle = \sum_i n_i \int \psi_i^*(\vec{r}_1) f_1(\vec{r}_1) \psi_i(\vec{r}_1) \, d^3 r_1$$

$$+ \frac{1}{2} \int \rho_{\uparrow}(\vec{r}_1) [\rho(\vec{r}_2) g(\vec{r}_1, \vec{r}_2) \, d^3 r_2 + U_{\uparrow}(\vec{r}_1)] \, d^3 r_1$$

$$+ \frac{1}{2} \int \rho_{\downarrow}(\vec{r}_1) [\rho(\vec{r}_2) g(\vec{r}_1, \vec{r}_2) \, d^3 r_2 + U_{\downarrow}(\vec{r}_1)] \, d^3 r_1$$

$$(2.2)$$

where

$$f_1(\vec{r}_1) = -\nabla_1^2 - \frac{2Z}{|\vec{r}_1|} \tag{2.3}$$

$$g(\vec{r}_1, \vec{r}_2) = \frac{2}{|\vec{r}_1 - \vec{r}_2|} \tag{2.4}$$

Here we have used the atomic units. Atomic units will be used throughout the paper unless otherwise specified. The first term in the expression for total energy is the expectation value of one-electron operators. The other terms are due to the interaction of an electron with the electron cloud. These interactions are spin dependent because of the exchange effect, so two separate terms are written for the two spins. The term $U_\sigma(\vec{r}_1)$ removes the self interaction term from the coulomb interaction and takes into account the exchange effect. As mentioned earlier, $U_\sigma(\vec{r}_1)$ is in general nonlocal. Slater has introduced a statistical approximation which has come to be known as exchange correlation potential or Xα potential.

The form for $U_\sigma(\vec{r}_1)$ in Slater approximation is

$$U_\sigma(\vec{r}_1) = U_{X\alpha\sigma}(\vec{r}_1) = -9\alpha \ [\frac{3\rho_\sigma(\vec{r}_1)}{4\pi}]^{1/3} \qquad (2.5)$$

where α is a multiplicative factor that can be chosen in calculations to give good agreement with experiments. The functional dependence of $U_{X\alpha}(\vec{r}_1)$ on $[\rho(\vec{r}_1)]^{1/3}$ is a consequence of the concept of a Fermi hole. This concept has been discussed by Slater.[27] With this form for $U_{X\alpha}(\vec{r}_1)$,

$$\langle E \rangle = \sum_i n_i \int \psi_i^*(\vec{r}_1) f_1(\vec{r}_1) \psi_i(\vec{r}_1) \ d^3r_1$$

$$+ \frac{1}{2} \int d^3r_1 \ d^3r_2 \ \rho(\vec{r}_1) g(\vec{r}_1,\vec{r}_2) \rho(\vec{r}_2)$$

$$+ \frac{\beta}{2} \int d^3r_1 \ [\rho_\uparrow^{4/3}(\vec{r}_1) + \rho_\downarrow^{4/3}(\vec{r}_1)] \qquad (2.6)$$

where

$$\beta = -9\alpha \ [\frac{3}{4\pi}]^{1/3} \qquad (2.7)$$

Thus $\langle E \rangle$ is a functional of occupation number n_i and spin orbitals ψ_i. One varies $\psi_i^*(\vec{r}_1)$ to minimize the total energy at fixed occupation number with the constraint

$$\int \psi_i^*(\vec{r}_1) \psi_i(\vec{r}_1) \ d^3r_1 = 1 \qquad (2.8)$$

Now the variational principle takes the form

$$\delta [<E> - n_i \, \varepsilon_i \int \psi_i^*(\vec{r}_1) \psi_i(\vec{r}_1) \, d^3 r_1] = 0 \qquad (2.10)$$

where ε_i is an undertermined Lagrange multiplier for the state i. The variation of $\psi_i^*(\vec{r}_1)$ gives

$$n_i \int \delta\psi_i^*(\vec{r}_1) [f_1(\vec{r}_1) + \int \rho(\vec{r}_2) g(\vec{r}_1, \vec{r}_2) d\vec{r}_2$$

$$+ \tfrac{2}{3}\beta/2 \, \rho_\sigma(1) - \varepsilon_i] \psi_i(\vec{r}_1) \, d^3 r_1 = 0 \qquad (2.11)$$

The orbital $\psi_i(\vec{r}_1)$ in the above equation refers to spin σ. For arbitrary variation $\delta\psi_i^*(\vec{r}_1)$, the term inside the bracket must vanish. This gives us the one-electron Schrodinger equation for spin σ.

$$[-\nabla_1^2 + V_c(\vec{r}_1) + V_{X\alpha\sigma}(\vec{r}_1)] \psi_i(\vec{r}_1) = \varepsilon_i \, \psi_i(\vec{r}_1)$$

$$(2.12)$$

For a rigorous derivation of this equation one is referred to the recent article of Rajagopal and Callaway[30] in which they have extended Kohn and Sham's formulation of the inhomogeneous paramagnetic electron gas problem to the

ferromagnetic and spin density wave systems. In the
present derivation

$$V_{X\alpha\sigma}(\vec{r}_1) = \frac{2}{3} U_{X\alpha\sigma}(\vec{r}_1) = -6\alpha \ [\frac{3\rho_\sigma(\vec{r}_1)}{4\pi}]^{1/3} \qquad (2.13)$$

In the paramagnetic system where one does not distinguish
the spin up electrons from the spin down electrons, one
has

$$V_{X\alpha}^{para}(\vec{r}_1) = -6\alpha \ [\frac{3\rho(\vec{r}_1)}{8\pi}]^{1/3} \ . \qquad (2.14)$$

The $\rho(\vec{r}_1)$ in the above equation refers to the total charge
density due to both the spin up and spin down electrons.
With the choice $\alpha=1$, we get the average exchange potential
which was first suggested by Slater in 1951. The choice
$\alpha=2/3$, gives the exchange potential suggested by Gaspar,
Kohn and Sham. Which one of these values of α is correct
in a band calculation has been a subject of controversy.
However, it is also to be observed that the values of
α lying between 1 and 2/3 and, in certain cases below
2/3, have given results which are in better agreement with
experiment than the results obtained with either $\alpha=1$ or
2/3 alone. The one-electron Schrödinger equation that is
appropriate for the paramagnetic case is

$$[-\nabla^2 + V_c(\vec{r}) + V_x(\vec{r})]\psi_i(\vec{r}) = \epsilon_i \, \psi_i(\vec{r}) \qquad (2.15)$$

where $\psi_i(\vec{r})$ are the one-electron wave functions. Previous calculations[20,21] on transition metals like Ni and Fe have shown that for self-consistent calculations a value of $\alpha=2/3$ or value very close to it gives better results than the value $\alpha=1$. With this in mind we choose $\alpha=2/3$ in the present calculation. Thus the average exchange potential is given by

$$V_x(\vec{r}) = -4 \, [\frac{3\rho(\vec{r})}{8\pi}]^{1/3} , \qquad (2.16)$$

and the Coulomb potential, $V_c(\vec{r})$ by

$$V_c(\vec{r}) = - \frac{2Z}{|\vec{r}|} + 2 \int \frac{\rho(\vec{r}')}{|\vec{r}-\vec{r}'|} \, d^3r' \qquad (2.17)$$

In the next two sections we shall discuss the solution of the one-electron Schrödinger equation with the exchange and Coulomb potentials given by Eqs. (2.16) and (2.17) respectively, to obtain $\psi_i(\vec{r})$ and ϵ_i.

Section II. Choice of Basis Set
and Construction of Crystal Potential

In this section we shall discuss the selection of a suitable set of basis functions which will be used to

evaluate the matrix elements of various operators occurring in the present calculation. We shall also discuss the method of construction of the one-electron potential occurring in the one-electron Schrödinger equation. This one electron potential is used in calculating the energy eigenvalues and eigenfunctions which serve as inputs to the first iteration of a self-consistency procedure.

In the conventional tight binding method one chooses a basis set of localized functions which are normalized, but which need not be orthogonal. These functions are usually chosen to be the one-electron atomic wave functions belonging to various symmetries. This is not necessary and may even be too restrictive. In our case some of the basis functions will be the atomic functions and others will be certain localized functions (Gaussian type functions). The basis functions, Φ_i, are now constructed as follows:

$$\Phi_i(\vec{k},\vec{r}) = \frac{1}{\sqrt{N}} \sum_{\vec{R}_\mu} e^{i\vec{k}\cdot\vec{R}_\mu} u_i(\vec{r}-\vec{R}_\mu) \qquad (2.18)$$

In the equation above N is the total number of atoms in the crystal. The functions u_i are localized at lattice sites described by the lattice vector $\vec{R}_\mu$. The wave vector $\vec{k}$ lies inside the first Brillouin unless stated otherwise. In this form, the set of function $\Phi_i(\vec{k},\vec{r})$ satisfy Bloch's

theorem.

The set of functions $u_i(\vec{r})$ are chosen to be the atomic wave functions representing 1s, 2s, 3s, 4s, 2p, 3p, 4p, and 3d states. The inclusion of core wave functions is necessary to avoid convergence difficulties associated with the non-orthogonality of the wave functions on different lattice sites.

There has been some evidence indicating that the d wave functions inside the solid are considerably different from the free atom d-wave functions. Thus one has to take special care in treating the d-wave functions inside the solid. All atomic functions except 3d functions were expressed as linear combinations of Gaussian type orbitals (GTO). Following Wachters,[31] s and p atomic functions were expressed as linear combinations of 14 and 11 GTO respectively. Five separate radial GTO's were used to represent each symmetry of d-functions. The orbital exponents of these radial functions describing the 3d electrons were taken to be the same as given by Wachters.

The basis set $\Phi_i(\vec{k},\vec{r})$ thus consists of 38 functions: 4 for s-symmetry (1s, 2s, 3s, 4s), 9 for p-symmetry $(2p_x, 2p_y, 2p_z, 3p_x, 3p_y, 3p_z, 4p_x, 4p_y, 4p_z)$ and 25 for d-symmetry (xy, yz, zx, x^2-y^2, $3z^2-r^2$). The atomic functions $u_i(\vec{r})$ can be written as

$$u_i(\vec{r}) = u_{n\ell m}(\vec{r}) = [\text{Angular Function}] \times R_{n\ell}(r)$$

The radial wave function $R_{n\ell}(r)$ is now expressed as the linear combination of GTO.

$$R_{n\ell}(\vec{r}) = \sum_{i} C_{n\ell i} \; N_{\ell i} \; r^{\ell-1} \; e^{-\alpha_{\ell i} r^2} \tag{2.19}$$

where the normalization constants $N_{\ell i}$ are given by

$$N_{\ell i} = [\sqrt{2}/\pi \; \frac{2^{2\ell+1} \alpha_{\ell i}^{(\ell+1)/2}}{(2\ell-1)!!}]^{1/2} \tag{2.20}$$

In the above expression, n is the principal quantum number, ℓ is the symmetry type index ($\ell=1,2,3$ for s,p,d-type symmetries respectively). The value of coefficients $C_{n\ell i}$ and $\alpha_{\ell i}$ are tabulated by Wachters,[31] obtained from a self-consistent field atomic calculation. The GTO's have been criticized because they have zero slope at the origin and becuase they decay too rapidly for large r. In a solid the second problem may not be as serious as in the case of a free atom, since the large distance behavior is strongly modified by the overlap of functions based on different sites. They have a major advantage over other functions, such as Slater type orbitals in that all necessary matrix elements can be calculated analytically in closed form. This saves much computing time and more than compensates for the larger number of GTO required to represent physical wave functions.

Next, we discuss the construction of the initial one-electron potential. The structure of the chromium crystal is a body centered cubic lattice. The neutral chromium

atom is taken to be in $3d^5 4s^1$ configuration. The configuration is used to calculate the spherically symmetric atomic charge densities. A superposition of these atomic charge densities are assumed to represent the charge density of the electrons inside the crystal. The crystal potential is calculated from these superposed charge densities. This would make the crystal potential dependent on a particular choice of the atomic configuration. It may seem logical to choose the ground state configuration of the atom, but this does not seem to be the best choice. (The ground state configuration of the chromium atom is $3d^4 4s^2$). The effective occupation number of orbitals of different symmetries may change in going from free atom to crystalline environment. The reason for this is, that when the atoms are brought together as in a crystal the sharp atomic levels broaden into bands. If the bands overlap the electron from one band will effectively go into another band changing the occupation number of the orbitals. However, if one performs a self-consistent calculation, the starting atomic configuration is in principle immaterial. The effect of different starting atomic configurations on the results of a non-self consistent band calculation has been illustrated in the work of Matheiss.[32] The crystal potential constructed from crystal charge density (superimposed atomic charge density) which has the symmetry of the crystal about any

lattice site will also have the symmetry of the lattice. The Coulomb part of the crystal potential can be expressed as

$$V_c(\vec{r}) = \sum_{R_\mu} v_a(\vec{r} - \vec{R}_\mu) \qquad (2.21)$$

where $v_a(\vec{r} - \vec{R}_\mu)$ is the potential at the point r, due to an atom centered at lattice site $\vec{R}_\mu$. In terms of charge density $\rho_a(r)$

$$v_a(\vec{r}) = -\frac{2Z}{r} + 2 \int \frac{\rho_a(\vec{r}_1) d^3 r_1}{|\vec{r} - \vec{r}_1|} , \qquad (2.22)$$

Z is the atomic number of the element under consideration (Z=24), for chromium). The factor 2, expresses the energy in Rydberg (atomic) units.

The spherically averaged charge density $\rho_a(r)$ is given as

$$\rho_a(r) = \frac{1}{4\pi} \sum_i n_i |R_i(r)|^2$$

$$= \frac{1}{4\pi} [2|R_{1s}(r)|^2 + 2|R_{2s}(r)|^2 + 2|R_{3s}(r)|^2$$

$$+ 1|R_{4s}(r)|^2 + 6|R_{2p}(r)|^2 + 6|R_{3p}(r)|^2$$

$$+ 5|R_{3d}(r)|^2] \qquad (2.23)$$

where $R_i(r)$ are the radial part of the atomic wave functions defined by Eq. (2.19).

As we shall shortly see, the Fourier coefficient of the crystal potential directly enters into the modified

tight binding calculation. The crystal potential is expanded in a Fourier series:

$$V(\vec{r}) = \sum_{\vec{K}} e^{i\vec{K}\cdot\vec{r}} V(\vec{K}_s) \qquad (2.24)$$

which can be inverted to obtain

$$V(\vec{K}) = \frac{1}{N\Omega} \int e^{-i\vec{K}\cdot\vec{r}} V(\vec{r}) \, d^3r \ . \qquad (2.25)$$

Let us first consider the evaluation of Fourier coefficients of Coulomb part of the crystal potential.

$$
\begin{aligned}
V_c(\vec{K}) &= \frac{1}{N\Omega} \int e^{-i\vec{K}\cdot\vec{r}} V_c(\vec{r}) \, d^3r \\[2mm]
&= \frac{1}{N\Omega} \sum_{\vec{R}_\mu} e^{-i\vec{K}\cdot\vec{r}} v_a(\vec{r}-\vec{R}_\mu) \, d^3r \\[2mm]
&= \frac{1}{N\Omega} \sum_{\vec{R}_\mu} e^{-i\vec{K}\cdot\vec{R}_\mu} \int d^3r \, e^{-i\vec{K}\cdot(\vec{r}-\vec{R}_\mu)} v_a(\vec{r}-\vec{R}_\mu)
\end{aligned}
$$

$$(2.26)$$

Using the relation

$$\sum_{\vec{R}_\mu} e^{-i\vec{K}\cdot\vec{R}_\mu} = N \sum_{\vec{K}_s} \delta_{\vec{K},\vec{K}_s}$$

where Ω is the volume of the primitive cell and $\vec{K}_s$ are reciprocal lattice vectors. Substituting for $v_a(\vec{r})$ from

Eq. (2.19) and using

$$\int \frac{e^{-i\vec{K}_s \cdot \vec{r}_2}}{|\vec{r}_1 - \vec{r}_2|} d^3 r_2 = \frac{4\pi}{K_s^2} e^{-i\vec{K}_s \cdot \vec{r}_1}$$

we have

$$V_c(K_s) = \frac{-8\pi Z}{\Omega K_s^2} + \frac{32\pi^2}{\Omega K_s^3} \int_0^\infty \rho_a(r) \sin(K_s r) r \, dr \quad (2.27)$$

In Eq. (2.27), $\rho_a(r)$ defined in Eq. (2.23) is used. This integral is easily evaluated. From the above equation we see that $V(K_s)$ is a function of $|K_s|$ only. Now we consider the limit of $V(\vec{K}_s)$ for $\vec{K}_s = 0$. Expanding the sine term in the integrand and taking the limit, we obtain

$$V_c(0) = \lim_{K_s \to 0} \left[-\frac{8\pi Z}{\Omega K_s^2} + \frac{8\pi Z}{\Omega K_s^3} \int_0^\infty \sum_i n_i |R_i(r)|^2 \right.$$

$$\left. \{K_s r - \frac{(K_s r)^3}{3!} + \ldots \ldots \} r \, dr \right.$$

$$= -4\pi/3\Omega \int_0^\infty \sum_i n_i |R_i(r)|^2 r^4 \, dr \quad (2.28)$$

Next, we turn our attention to construction of exchange potential. As discussed in the first section of this chapter, the true Hartree-Fock exchange operator is taken as an average exchange operator that is the same for all states. This exchange potential is

$$V_x(\vec{r}) = -6\alpha \ [\frac{3\rho(\vec{r})}{8\pi}]^{1/3}$$

where $\alpha=\frac{2}{3}$ is used in the present calculation. With this choice for $V_x(\vec{r})$, the Fourier coefficients of exchange potential are given by

$$V_x(\vec{K}_s) = \frac{-4\pi}{\Omega} \ \frac{6\alpha}{K_s} \int_0^\infty \ [\frac{3\rho(r)}{8\pi}]^{1/3} r \ \sin(K_s r) dr$$

$$(2.29)$$

The presence of $[\rho(r)]^{1/3}$ in the integrand does not permit us to evaluate the integral analytically as was done for the coulomb potential. One has to resort to a numerical method to evaluate this integral. The following assumption is made in evaluating this integral. The region of integration is replaced by a sphere centered around an atom. This sphere is chosen to have the same volume as the primitive cell. The charge densities are calculated at chosen points along the radii in three independent directions. These charge densities are the superposition of charge densities arising from the neighboring atoms. Contributions from atoms from different cells are taken until converged values for the charge densities are obtained. With this numerical charge density, a 96 point Gaussian formula is used to carry out the integration for different values of K_s.

Section III. Description of the Tight Binding Method

The tight binding or LCAO (Linear Combination of Atomic Orbitals) method was introduced by Bloch in 1928. This method of band calculation, however, had fallen into bad repute because one could not make it quantitative. This was because the three center integrals occurring in the LCAO method were difficult to evaluate. They were either neglected completely or some crude approximations w e r e m a d e. A technique has recently been developed by Lafon and Lin[19] (1966) which does not require an evaluation of these three center integrals. To see how the three center integrals come about in the old tight binding method, one just needs to look at the matrix element of the Coulomb potential. The matrix element is given by

$$< \Phi_i(\vec{k}, \vec{r}) \,|\, V_c(\vec{r}) \,|\, \Phi_j(\vec{k}, \vec{r}) >$$

$$= \frac{1}{N} \sum_{R_\mu, R_\rho, R_\lambda} e^{i\vec{k} \cdot (\vec{R}_\rho - \vec{R}_\mu)} \int d^3r \ u_i^*(\vec{r} - \vec{R}_\mu) v_a(\vec{r} - \vec{R}_\lambda)$$

$$u_j(\vec{r} - \vec{R}_\rho) \tag{2.30}$$

where we have used Eq. (2.21) for $V_c(r)$. This matrix element thus involves three center integrals. One can overcome this difficulty by making a Fourier expansion of the crystal potential as will be shown below.

The equation to be solved is the one-electron Schrodinger equation which has been discussed in Section I of this chapter.

$$H \, \psi_n(\vec{k},\vec{r}) = E_n(\vec{k}) \, \Psi_n(\vec{k},\vec{r}) \qquad (2.31)$$

where H is the Hamiltonian appearing in Eq. (2.12). $\psi_i(\vec{r})$ are now written with all the indices. The basis set $\Phi_i(k,r)$ discussed in the last section is used to calculate the matrix elements of the Hamiltonian operator and the overlap matrix elements. The set consisting of only the atomic states does not form a complete set, so an expansion of the wave function using this set as a basis does not lead to an exact solution of the Schrödinger equation. However, inclusion of all the bound states and some excited states can be expected to be a fair approximation to the actual wave function. The crystal wave function $\psi_n(\vec{k},\vec{r})$ is expressed as

$$\psi_n(\vec{k},\vec{r}) = \sum_i a_{ni}(\vec{k}) \, \phi_i(\vec{k},\vec{r})$$

$$= \frac{1}{\sqrt{N}} \sum_{i,\vec{R}_\mu} e^{i\vec{k}\cdot\vec{R}_\mu} a_{ni}(\vec{k}) \, u_i(\vec{r}-\vec{R}_\mu) \qquad (2.32)$$

where n is the band index, and $\vec{k}$ is the electron wave fector limited to the first Brillouin Zone. The

coefficients $a_{ni}(k)$ are to be determined by diagonalizing Eq. (2.31). Substituting Eq. (2.32) in Eq. (2.31) and taking the expectation value we obtain a secular determinant for every $\vec{k}$ inside the Brillouin Zone

$$\text{Det} \left| H_{mn}(\vec{k}) - E(\vec{k}) O_{mn}(\vec{k}) \right| = 0 \qquad (2.33)$$

where

$$H_{mn}(\vec{k}) = \sum_{\vec{R}_\mu} e^{i\vec{k} \cdot \vec{R}_\mu} \int u_m^*(\vec{r} - \vec{R}_\mu) [-\nabla^2 + V(\vec{r})] u_n(\vec{r}) \, d^3r$$

$$= T_{mn}(\vec{k}) + V_{mn}(\vec{k}) . \qquad (2.34)$$

The crystal potential $V(\vec{r})$ consists of the Coulomb and exchange parts and was discussed in detail in the last section. In the tight binding method modified by Lafon and Lin, the crystal potential is expanded in terms of the reciprocal lattice vectors:

$$V(\vec{r}) = \sum_{\vec{K}} e^{i\vec{K} \cdot \vec{r}} V(\vec{K})$$

$$= \sum_{\vec{K}} e^{i\vec{K} \cdot \vec{r}} [V_c(\vec{K}) + V_x(\vec{K})] .$$

Then,

$$V_{mn}(\vec{k}) = \sum_{\vec{R}_\mu} e^{-i\vec{k}\cdot\vec{R}_\mu} \int u_m^*(\vec{r}-\vec{R}_\mu)\, [\sum_{\vec{K}} e^{i\vec{K}\cdot\vec{r}}\{V_C(\vec{K})+V_X(\vec{K})\}$$

$$\times\, u_n(\vec{r})\, d^3r$$

$$= \sum_{\vec{R}_\mu} e^{-i\vec{k}\cdot\vec{R}_\mu} \sum_{\vec{K}} [V_C(\vec{K})+V_X(\vec{K})]\, S_{mn}(\vec{K},\vec{R}_\mu)\ ,$$

$$(2.35)$$

where

$$S_{mn}(\vec{K},\vec{R}_\mu) = \int d^3r\, e^{i\vec{K}\cdot\vec{r}}\, u_m^*(\vec{r}-\vec{R}_\mu) u_n(\vec{r})\ . \qquad (2.36)$$

For a crystal having a center of inversion, $e^{i\vec{K}\cdot\vec{r}}$ in the above equation can be replaced by $\cos(\vec{K}\cdot\vec{r})$. We also have

$$O_{mn}(\vec{k}) = \sum_{\vec{R}_\mu} e^{-i\vec{k}\cdot\vec{R}_\mu} \int d^3r\, u_m^*(r) u_n(\vec{r}-\vec{R}_\mu) \qquad (2.37)$$

and

$$T_{mn}(\vec{k}) = \sum_{\vec{R}_\mu} e^{-i\vec{k}\cdot\vec{R}_\mu} \int d^3r\, u_m^*(\vec{r}-\vec{R}_\mu)\, (-\nabla^2) u_n(\vec{r})$$

$$(2.38)$$

As seen from these equations, the calculation of matrix elements $S_{mn}(\vec{K},\vec{R}_\mu)$ is fundamental to the tight binding method. These matrix elements can be calculated analytically when the atomic functions are expressed as linear combination of GTO. It is difficult to express these matrix elements in a closed form when the atomic functions are expressed in terms of the Slater type orbitals. This was the reason for choosing the GTO in the expansion of the atomic functions.

The integrals $S_{mn}(\vec{K},\vec{R}_\mu)$ for arbitrary orbitals m,n can be determined from 1s-1s (m,n referring 1s orbitals) integrals by suitable differentiation. We shall evaluate this integral for 1s-1s orbitals as an example. The co-ordinates of various points are shown in Fig. II. We choose the special case where $\vec{C}$ and $\vec{A}$ are at the origin. The vector $\vec{R}_\mu$ is taken as the vector $\vec{R}_B$. In terms of the GTO, the integral (2.36) for 1s-1s orbital pairs can now be written as

$$S_{1s-1s}(\vec{K},\vec{R}_\mu) = \sum_{i,j} D(i,j;1s,1s) \int e^{-(\alpha_i r^2 + \alpha_j r_\mu^2)}$$
$$\cos(\vec{K}\cdot\vec{r})\, d^3r \qquad (2.39)$$

where

$$\vec{r}_\mu = \vec{r} - \vec{R}_\mu \quad . \qquad (2.40)$$

$D(i,j;1s,1s)$ includes the angular normalization factors, the normalization $(N_{\ell i})$ arising from radial functions and the coefficients $c_{n\ell i}$ [see Eq. (2.19)]. The product of two Gaussians occurring in the integrand of Eq. (2.39) can be written in terms of another Gaussian as follows

$$e^{-(\alpha_i r^2 + \alpha_j r_\mu^2)} = e^{-\frac{(\alpha_i \alpha_j r_\mu^2)}{\alpha_i + \alpha_j}} e^{-(\alpha_i + \alpha_j) r_D^2}.$$

$$(2.41)$$

where the coordinates of the point D is given as

$$D_\gamma = \frac{\alpha_j (\vec{R}_\mu)}{\alpha_i + \alpha_j} \quad , \quad \gamma = x, y, z \qquad (2.42)$$

Writing

$$\vec{r} = \vec{D} + \vec{r}_D$$

the integral in Eq. (2.39) can be written as

$$\int e^{-(\alpha_i r^2 + \alpha_j r_\mu^2)} \cos \vec{K} \cdot \vec{r} \ d^3 r$$

$$= e^{-\frac{\alpha_i \alpha_j R_\mu^2}{\alpha_i + \alpha_j}} \cos \vec{K} \cdot \vec{D} \int e^{-(\alpha_i + \alpha_j) r_D^2} \cos(\vec{K} \cdot \vec{r}_D) d^3 r_D.$$

$$(2.43)$$

The integral is easily evaluated and the final result for $S_{1s-1s}(\vec{K}, \vec{R}_\mu)$ can be written as

$$S_{1s-1s}(\vec{K}, \vec{R}_\mu) = \sum_{i,j} D(i,j;1s,1s) \ [\frac{\pi}{\alpha_i + \alpha_j}]^{3/2}$$

$$e^{-\frac{\alpha_i \alpha_j}{\alpha_i + \alpha_j} R_\mu^2} e^{-K^2/4(\alpha_i + \alpha_j)} \cos(\vec{K} \cdot \vec{D}) \qquad (2.44)$$

The integrals involving orbitals of different symmetry are given in the Appendix A along with expressions for the kinetic energy integrals defined in Eq. (2.38).

For a given $\vec{k}$ in the Brillouin Zone, all matrices are of dimension 38x38. As mentioned earlier, the computation of the matrix elements of the Hamiltonian, $H_{mn}(\vec{k})$, involves both the sums over the direct and the reciprocal lattice vectors. Both of these sums must be carried out until convergence is reached. The problem of convergence depends on the types of the orbitals appearing in the matrix elements. The matrix elements with the symmetry pairs s-s, s-p, p-p converged rather slowly. For example, in the s-s type of the matrix elements, for the first five neighbors in the direct space, 12,000 rotationally independent reciprocal lattice vectors were required to obtain convergence up to a certain level. However, this convergence was not complete, so the remainder of the sum over the reciprocal lattice vectors was approximated by an integration. The matrix elements involving d-type orbitals converged quite rapidly, however. With these calculated matrix elements, the secular equation, (2.31), is solved to obtain the coefficients $a_{ni}(\vec{k})$ and the energy eigenvalues $E_n(\vec{k})$ at 55 $\vec{k}$ points in 1/48th of the Brillouin Zone. These eigenfunctions served as the input to the first iteration of a self-consistency procedure.

The eigenvalues and eigenfunctions obtained at this stage were not self-consistent because the potential from which they were derived was a superposition of atomic potentials. The next step then was to make the calculation self-consistent.[22] This is accomplished through an iterative procedure. At any given iteration a potential was constructed from the band wave functions calculated in the previous iteration. This new potential was again used to calculate a newer set of wavefunctions. This process was repeated until convergence was achieved.

The charge density $\rho(\vec{r})$ from which the crystal potential was constructed is expressed as

$$\rho(\vec{r}) = \sum_{\substack{n,\vec{k} \\ occu.}} |\psi_n(\vec{k},\vec{r})|^2 \qquad (2.45)$$

where the sum is over the occupied states of the band. Since in this calculation one needs the Fourier coefficient of the potential, the iterated values of $V(\vec{K})$ were computed. For $\vec{K} \neq 0$, the Fourier coefficient of the Coulomb potential is given as

$$V_c(\vec{K}) = -8\pi \frac{\rho(\vec{K})}{K^2} \qquad (2.46)$$

where $\rho(\vec{K})$ is related to the charge density via

$$\rho(\vec{K}) = \frac{1}{N\Omega} \int e^{-i\vec{K}\cdot\vec{r}} \rho(\vec{r}) \, d^3r \; . \qquad (2.47)$$

Substituting for $\rho(\vec{r})$ from Eq. (2.45) in Eq. (2.47) one obtains

$$\rho(\vec{K}) = \frac{1}{(2\pi)^3} \sum_{n,i,j} \int d^3k \; a^*_{ni}(\vec{k}) \; a_{nj}(\vec{k})$$

$$[\sum_{\vec{R}_\mu} e^{i\vec{k}\cdot\vec{R}_\mu} S_{ij}(\vec{K},\vec{R}_\mu)] \; . \qquad (2.48)$$

The expression inside the square bracket is a generalized overlap matrix element (for $\vec{k}=0$, one has the usual overlap matrix elements). The integration d^3k is over the occupied region of the Brillouin Zone and $S_{ij}(\vec{K},\vec{R}_\mu)$ were defined in Eq. (2.36). If a fixed set of basis functions are used one needs to compute the quantities in the square brackets of Eq. (2.48) only once. For the case $\vec{K}=0$, one takes the limit of the Eq. (2.48), and obtains

$$V_c(0) = \frac{1}{6\pi^2} \sum_{\substack{i,j \\ n}} \int d^3k \; a^*_{ni}(\vec{k}) \; a_{nj}(\vec{k}) \; S^{(2)}_{ij}(\vec{k})$$

$$(2.49)$$

where

$$S^{(2)}_{ij}(\vec{k}) = \sum_{\vec{R}_\mu} e^{i\vec{k}\cdot\vec{R}_\mu} \int u^*_i(\vec{r}) r^2 u_j(\vec{r}-\vec{R}_\mu) \; d^3r \qquad (2.50)$$

The calculation of the corrected exchange potential coefficients was more cumbersome because a spherically symmetric charge density had to be reconstructed numerically at 96 points inside the sphere of equal volume

to the unit cell. The change in the Fourier coefficients
of the charge density [see Eq. (2.48) and Eq. (2.47)] was
averaged over directions of the reciprocal lattice vector
$\vec{K}$ and the change in charge density, $\Delta\rho(\vec{r})$

$$\Delta\rho(\vec{r}) = \sum_{\vec{K}} \Delta\rho(\vec{K}) e^{i\vec{K}\cdot\vec{r}} \tag{2.51}$$

was numerically determined. This change was added to the
starting charge density. The charge density thus ob-
tained was used to calculate the Fourier coefficient of
the exchange potential. The change in the Coulomb and
exchange potential Fourier coefficients were added to the
Hamiltonian matrix element in the following way

$$H_{ij}(\vec{k}) = H^{O}_{ij}(\vec{k}) + \sum_{\vec{K}} \Delta V(\vec{K}) \; [\sum_{\vec{R}_{\mu}} e^{i\vec{k}\cdot\vec{R}_{\mu}} \; S_{ij}(\vec{K},\vec{R}_{\mu})] \tag{2.52}$$

where

$$\Delta V(\vec{K}) = \Delta V_{c}(\vec{K}) + \Delta V_{x}(\vec{K}) \; , \tag{2.53}$$

The $H_{ij}(\vec{k})$ were the Hamiltonian matrix elements at a
given stage of the iteration and $H^{O}_{ij}(\vec{k})$ were matrix
elements of the original Hamiltonian defined in Eq.
(2.34). The Hamiltonian $H_{ij}(\vec{k})$ was again diagonalized to

to obtain a new set of eigenfunctions and eigenvalues.
The process was repeated till convergence was achieved.

Only the smallest 20 rotationally independent Fourier
coefficients of the crystal potential changed significantly
in the self-consistency process. The Fourier coefficients
corresponding to large values of $\vec{k}$ describe the core
charge densities and were not affected by self-consistency
procedure. The criterion used to define an adequate
degree of self-consistency was that the Fourier co-
efficients of the Coulomb potential be stable to within
0.001 Ryd. Eleven iterations were necessary to achieve
self-consistency. The first four iterations were based
on the wave functions obtained at 14 inequivalent points
in 1/48th of the Brillouin Zone. The final seven
iterations employed 55 points. The exchange potential
was found to converge more rapidly than the Coulomb
potential. The Fourier coefficients of the exchange and
Coulomb potentials for the first twenty reciprocal lattice
vectors are listed in Table I. With the self-consistent
potential thus obtained, the energy eigenvalues and
eigenfunctions were calculated at 819 points in 1/48th of
the Brillouin Zone. These eigenfunctions were used to
calculate the X-ray form factor and Compton profile. A
brief discussion of the Compton profile will be given in
the next chapter.

CHAPTER III: THE COMPTON PROFILE

Following the discovery and explanation of Compton effect, it was suggested by several authors that X-ray scattering from the electrons in the solid could yield valuable information about their linear momentum distribution in the ground state. Yet only recently have such experiments been carried out with sufficient accuracy to bring out these interesting features of the momentum distribution. Unlike X-ray scattering factor measurements, Compton scattering measurements are sensitive to the outer electrons and can simply be related to the momentum distribution of the outer electrons. Thus it has been suggested that Compton scattering experiments can provide a crucial test for the wavefunctions obtained from energy band calculations.[37,38,39]

The theory of the Compton line shape in the impulse approximation was first given by Platzman and Tzoar.[33] The impulse approximation is valid only if i) the photons interact with a single electron, and ii) the binding forces between the ejected electron and the other particles in the system are essentially constant during the time of collision. We shall outline the derivation of Compton line shape following Platzman and Tzoar[33] in order to bring out these approximations.

In the Born approximation, one can calculate the differential scattering cross section for a process in which an incident photon is inelastically scattered by a many electron system. If the incident photon has energy $h\omega_1$, wave vector $\vec{k}_1$ and polarization $\hat{\epsilon}_1$ and the scattered photon has energy ω_2, wave vector $\vec{k}_2$ and polarization $\hat{\epsilon}_2$, then the differential Compton scattering cross section is

$$\frac{d^2\sigma}{d\Omega d\omega} = \left(\frac{e^2}{mc^2}\right)^2 (\hat{\epsilon}_1 \cdot \hat{\epsilon}_2)^2 \frac{\omega_2}{\omega_1} S(\vec{k},\omega) \ . \qquad (3.1)$$

This is well known and may be found, for instance, in Ref. (35).

In the above derivation, the contribution of $\vec{p} \cdot \vec{A}$ term which arises from coupling of the electromagnetic field with the matter field has been neglected. The contribution to the cross section is mainly from the A^2 term in the interaction Hamiltonian. The ratio of the contribution from the A^2 term to the $\vec{p} \cdot \vec{A}$ term is of the order of $\hbar\omega_1/mc^2$. Further considerations show that this formula to be valid for $\omega_1 \gg \omega_p$, and $E_F \ll \hbar\omega_1 \ll mc^2$, ($\omega_p$ is the plasma frequency). In Eq. (3.1), $\vec{k}=\vec{k}_1-\vec{k}_2$, the momentum transfer of the photon, and $\omega=\omega_1-\omega_2$. The structure factor $S(\vec{k},\omega)$ is given by

$$S(\vec{k},\omega) = \frac{1}{2\pi} \int_{-\infty}^{+\infty} <n_{\vec{k}}(t)\,n_{-\vec{k}}(0)>e^{i\omega t} \qquad (3.2)$$

$$n_{\vec{k}}(t) = \sum_{\vec{p}} a^{+}_{\vec{k}+\vec{p}}(t)\,a_{\vec{p}}(t) \qquad (3.3)$$

a^{+}_k, a_k are the electron creation and annihilation operators respectively. Expression (3.3) refers to an electron gas and will be modified appropriately later for the Bloch electrons. The angular bracket is the ensemble average over the initial state of the many electron system. In our case the initial state of the system is the ground state at zero temperature. Eq. (3.1) can be rewritten as

$$\frac{d^2\sigma}{d\Omega d\omega} = (\frac{e^2}{mc^2})^2 \frac{\omega_2}{\omega_1} (\hat{\epsilon}_1 \cdot \hat{\epsilon}_2) \frac{1}{2\pi} \int_{-\infty}^{+\infty} e^{i\omega t} \sum_{\vec{p},\vec{p}'}$$

$$<a^{+}_{\vec{p}}(t)\,a_{\vec{p}-\vec{k}}(t)\; a^{+}_{\vec{p}'-\vec{k}}\, a_{\vec{p}'}> \qquad (3.4)$$

Henceforth we shall use $n_{\vec{p}}$ to denote the number operator.

It is assumed that for the ground state of the interacting electron gas, $n_{\vec{p}} = <a^{+}_{\vec{p}}a_{\vec{p}}>$ is finite only for $\vec{p}$ of the order of p_F. The wave vector of the photon is taken to be so large that $n_{\vec{p}-\vec{k}}=0$. In Eq. (3.4) the operator $a^{+}_{\vec{p}}$ operates directly to the left on the ground state of the system. The operator $a_{\vec{p}'}$ operates directly to the right on the ground state of the system. This implies that both $\vec{p}$, and $\vec{p}'$ are of order of magnitude of P_F, the Fermi momentum.

By our assumption on $\vec{k}$,

$$|\vec{p}-\vec{k}| >> P_F \quad , \quad |\vec{p}'-\vec{k}| >> P_F \ .$$

Further, it is assumed that

$$a_{\vec{p}-\vec{k}}(t) = a_{\vec{p}-\vec{k}} \ e^{-i\varepsilon_{\vec{p}-\vec{k}}t} \tag{3.5}$$

i.e., the fast particle behaves like a free particle. The energy $\varepsilon_{\vec{p}-\vec{k}}$ is given by

$$\varepsilon_{\vec{p}-\vec{k}} = (\vec{p}-\vec{k})^2/2m \tag{3.6}$$

In writing Eq. (3.5) the interaction between the fast particle and the rest of the system was neglected.

Using Eq. (3.5) we can write the correlation function occurring in Eq. (3.4) as

$$<a_{\vec{p}}^+(t) a_{\vec{p}-\vec{k}}(t) a_{\vec{p}'-\vec{k}}^+ a_{\vec{p}'}>$$

$$\underset{\sim}{=} e^{-i\varepsilon_{\vec{p}-\vec{k}}t} <a_{\vec{p}}^+(t) a_{\vec{p}'} a_{\vec{p}-\vec{k}} a_{\vec{p}'-\vec{k}}^+> \tag{3.7}$$

The operator $a_{\vec{p}-\vec{k}}^+$ operating on the ground state of the interacting system creates with unit probability an electron of momentum $\vec{p}-\vec{k}$, since by the assumption on magnitude of $\vec{k}$, the state $\vec{p}-\vec{k}$ is unoccupied. The operator

$a_{\vec{p}-\vec{k}}^{}$ must annihilate with unit probability this high

energy particle so that the matrix element vanishes unless

$\vec{p}'=\vec{p}$. Thus, one obtains

$$\langle a_{\vec{p}}^{+}(t)\, a_{\vec{p}-\vec{k}}^{+}(t)\, a_{\vec{p}'-\vec{k}}^{+}\, a_{\vec{p}'}^{}\rangle = \langle a_{\vec{p}}^{+}(t)\, a_{\vec{p}}^{}\rangle\, e^{-i\epsilon_{\vec{p}-\vec{k}}t}\, \delta_{\vec{p},\vec{p}'}$$

$$(3.8)$$

Substituting Eq. (3.9) in Eq. (3.4)

$$\frac{d^2\sigma}{d\Omega d\omega} = (\frac{e^2}{mc^2})^2\, (\hat{\epsilon}_1\cdot\hat{\epsilon}_2)^2\, \frac{\omega_2}{\omega_1}\, \sum_{\vec{p}}\, \int_{-\infty}^{+\infty} \frac{dt}{2\pi}\, e^{i\omega t}\, e^{-i\epsilon_{\vec{p}-\vec{k}}t}$$

$$\langle a_{\vec{p}}^{+}(t)\, a_{\vec{p}}^{}\rangle \qquad\qquad (3.9)$$

If one neglects the time dependence of the operator $a_{\vec{p}}^{+}(t)$

in Eq. (3.9), an error of the order $p^2/2m$ relative to

$k^2/2m$ is introduced. To be consistent then one writes

$$\epsilon_{\vec{p}-\vec{k}} = k^2/2m - \frac{\vec{k}\cdot\vec{p}}{m}$$

so that Eq. (3.8) can be written as

$$\frac{d^2\sigma}{d\Omega d\omega} = (\frac{e^2}{mc^2})^2\, (\hat{\epsilon}_1\cdot\hat{\epsilon}_2)^1\, \frac{\omega_2}{\omega_1}\, \sum_{\vec{p}}\, \delta[\frac{k^2}{2m} - \frac{\vec{k}\cdot\vec{p}}{m} - \omega]\, \langle a_{\vec{p}}^{+}a_{\vec{p}}^{}\rangle$$

$$= (\frac{e^2}{mc^2})^2\, (\hat{\epsilon}_1\cdot\hat{\epsilon}_2)^2\, \frac{\omega_2}{\omega_1}\, \int \frac{d^3p}{(2\pi)^3}\, n_{\vec{p}}\, \delta[\frac{k^2}{2m} - \omega - \frac{\vec{k}\cdot\vec{p}}{m}]$$

$$= r_o^2 (\hat{\epsilon}_1 \cdot \hat{\epsilon}_2)^2 \frac{\omega_2}{\omega_1} \cdot \frac{m}{|k|} \cdot \frac{1}{(2\pi)^3} \int n(\vec{p}) \delta [\frac{k}{2} - \frac{m\omega}{k}$$

$$- \frac{\vec{k} \cdot \vec{p}}{k}] \, d^3p \qquad\qquad (3.10)$$

with

$$\frac{k}{2} - \frac{m\omega}{k} = q \qquad\qquad (3.11)$$

and

$$\frac{\vec{k}}{k} = \hat{d}$$

$$\frac{d^2\sigma}{d\Omega d\omega} = r_o^2 (\hat{\epsilon}_1 \cdot \hat{\epsilon}_2) \frac{\omega_2}{\omega_1} \frac{m}{|\vec{k}|} \cdot \frac{1}{(2\pi)^3} J(q) \qquad\qquad (3.12)$$

where

$$J(q) = \int n(\vec{p}) \delta [q - \hat{d} \cdot \vec{p}] \, d^3p$$

In the derivation of Eq. (3.12) it is to be emphasized that the following approximations were made: (i) the wavelength of the incident photon is so large that it interacts with an individual electron and ejects it instantaneously from the Fermi sphere (large recoil energy). The rest of the system, that is, the remaining electrons and holes are left to evolve by themselves via their total Hamiltonian, and (ii) the recoil energy of

the electron is so large compared to its binding energy
that the binding energy can be completely neglected.
These approximations have come to be known as the impulse
approximation. The validity of the impulse approxima-
tion and its comparison with an exact calculation is
found in Ref. (34). The Compton profile $J(q)$, defined
in Eq. (3.12) must be properly normalized. The normaliza-
tion should be such that

$$\int_{-\infty}^{+\infty} J(q)\,dq = n_e \ ,$$

where n_e is the number of electrons in the unit cell.
This follows from the normalization of the wave function.
Write $J(q)$ as

$$J(q) = c \int d^3p \ n(\vec{p}) \ \delta[q - \hat{d}\cdot\vec{p}]$$

where c is to be determined. We now turn our attention
to the case of Bloch electrons. We define the Fourier
transform of the Bloch functions, $\psi_n(\vec{k},\vec{r})$,

$$\psi_n(\vec{k},\vec{p}) = \frac{1}{\sqrt{N\Omega}} \int e^{-i\vec{p}\cdot\vec{r}} \ \psi_n(\vec{k},\vec{r}) \ d^3r \ ,$$

where $\psi_n(\vec{k},\vec{r})$ are expressed as

$$\psi_n(\vec{k},\vec{r}) = \frac{1}{\sqrt{N}} \sum_{\vec{R}_\mu} \sum_i e^{i\vec{k}\cdot\vec{R}_\mu} a_{ni}(\vec{k}) u_i(\vec{r}-\vec{R}_\mu)$$

The $u_i(\vec{r}-\vec{R}_\mu)$ are the atomic orbitals (or the localized functions) situated at the lattice site $\vec{R}_\mu$. The co-efficients $a_{ni}(\vec{k})$ were obtained from the band structure calculation, Ω is the volume of the primite cell. The momentum distribution function, $n(\vec{p})$, is related to $\psi_n(\vec{k},\vec{p})$ through

$$n(\vec{p}) = \sum_{\substack{n,\vec{k} \\ occ.}} |\psi_n(\vec{k},\vec{p})|^2 \qquad (3.13)$$

thus

$$\int |\psi_n(\vec{k},\vec{p})|^2 d^3p = \frac{(2\pi)^3}{\Omega} \int_{cell} d^3r \, |\psi_n(\vec{k},\vec{r})|^2$$

Summing both the sides of the above equation over the occupied region of the Brillouin Zone,

$$\sum_{\substack{n,\vec{k} \\ occ.}} \int |\psi_n(\vec{k},\vec{p})|^2 \, d^3p = \int n(\vec{p}) d^3p = \frac{(2\pi)^3}{\Omega} \sum_{n,\vec{k}}$$

$$\int_{cell} d^3r \, |\psi_n(\vec{k},\vec{r})|^2$$

thus

$$\int n(\vec{p})d^3p = \frac{(2\pi)^3}{\Omega} \int_{cell} d^3r \; \rho(\vec{r}) = \frac{(2\pi)^3}{\Omega} n_e$$

but

$$\int_{-\infty}^{+\infty} J(q)dq = C \int_{-\infty}^{+\infty} dq \int d^3p \; n(\vec{p}) \; \delta[q-\hat{d}\cdot\vec{p}]$$

$$= C \int d^3p \; n(\vec{p})$$

Thus the properly normalized Compton profile is given by

$$J(q) = \frac{\Omega}{(2\pi)^3} \int d^3p \; n(\vec{p}) \; \delta[q-\hat{d}\cdot\vec{p}]$$

This equation can be rewritten as

$$J(q) = \frac{\Omega}{(2\pi)^3} \int d^3p \; \sum_{\substack{n,\vec{k} \\ \alpha}} \left| \frac{1}{\sqrt{N\Omega}} \int d^3r \; e^{-i\vec{p}\cdot\vec{r}} \right.$$

$$\left. \psi_n(\alpha\vec{k},\vec{r}) \right|^2 \; \delta[q-\hat{d}\cdot\vec{p}] \tag{3.14}$$

where α are the 48 operations of the cubic group, and $\vec{k}$ in the above equation is taken to be inside 1/48th of the Brillouin Zone. The effect of operations of the cubic group can be expressed as a unitary transformation of the Bloch functions, and since we are interested in the sum over the modulus squared of the wave function, we can write Eq. (3.14) as

$$J(q) = \frac{\Omega}{(2\pi)^3} \int d^3p \sum_{\substack{n,k \\ \alpha}} \frac{1}{\sqrt{N\Omega}} \int d^3r \, e^{-i\vec{p}\cdot\vec{r}}$$

$$\psi_n(\vec{k}, \alpha^{-1}\vec{r})|^2 \, \delta[q-\hat{d}\cdot\vec{p}]$$

$$= \frac{\Omega}{(2\pi)^3} \int d^3p \sum_{\substack{n,k \\ \alpha}} |\frac{1}{\sqrt{N\Omega}} \int d^3r \, e^{-i\vec{p}\cdot\alpha\vec{r}}$$

$$\psi_n(\vec{k},\vec{r})|^2 \, \delta[q-\hat{d}\cdot\vec{p}] \tag{3.15}$$

by suitable transformation Eq. (3.15) can be written as

$$J(q) = \frac{\Omega}{(2\pi)^3} \int d^3p \sum_{\substack{n,k \\ \alpha}} |\psi_n(\vec{k},\vec{p})|^2 \sum_{\alpha} \delta[q-\alpha^{-1}\hat{d}\cdot\vec{p}]$$

$$\tag{3.15'}$$

now $\psi_n(\vec{k},\vec{p})$ was defined as,

$$\psi_n(\vec{k},\vec{p}) = \frac{1}{\sqrt{N\Omega}} \int e^{-i\vec{p}\cdot\vec{r}} \, \psi_n(\vec{k},\vec{r}) \, d^3r$$

Substituting for $\psi_n(\vec{k},\vec{r})$ in the above equation we get

$$\psi_n(\vec{k},\vec{p}) = \frac{1}{\sqrt{N\Omega}} \frac{1}{\sqrt{N}} \sum_{R_\mu,i} a_{ni}(\vec{k}) e^{i\vec{k}\cdot\vec{R}_\mu} \int e^{-i\vec{p}\cdot\vec{r}}$$

$$u_i(\vec{r}-\vec{R}_\mu) d^3r$$

$$= \frac{1}{N} \sum_{R_\mu, i} a_{ni}(\vec{k}) e^{-i(\vec{k}-\vec{p}) \cdot \vec{R}_\mu} \frac{1}{\sqrt{\Omega}} \int e^{-i\vec{p} \cdot \vec{r}}$$

$$u_i(\vec{r}) \, d^3r \ .$$

Using the identity,

$$\sum_{\vec{R}_\mu} e^{i(\vec{k}-\vec{k}') \cdot \vec{R}_\mu} = N \sum_{\vec{K}_s} \delta_{\vec{k}, \vec{k}'+\vec{K}_s} \ ,$$

where $\vec{K}_s$ are reciprocal lattice vectors, we have

$$\psi_n(\vec{k}, \vec{p}) = \sum_i a_{ni}(\vec{k}) u_i(\vec{p}) \sum_{\vec{K}_s} \delta_{\vec{p}, \vec{k}+\vec{K}_s} \ , \tag{3.16}$$

where

$$u_i(\vec{p}) = \frac{1}{\sqrt{\Omega}} \int e^{-i\vec{p} \cdot \vec{r}} u_i(\vec{r}) \, d^3r \ . \tag{3.17}$$

The Fourier transform, $u_i(\vec{p})$, of the functions $u_i(\vec{r})$ are given in the Appendix B. Substitution of Eq. (3.16) in Eq. (3.15'), and converting the sum over $\vec{k}$ to an integral over the Brillouin Zone, we have finally

$$J(q) = \frac{\Omega}{(2\pi)^3} \sum_{n} \sum_{\vec{K}_s} \int_{\vec{k}, occ} d^3k \left| \sum_i a_{ni}(\vec{k}) u_i(\vec{k}+\vec{K}_s) \right|^2$$

$$\times \left[\sum_\alpha \delta[q - \alpha^{-1}\hat{d} \cdot (\vec{k}+\vec{K}_s)] \right] \tag{3.18}$$

This is the expression for the Compton profile which was used in our computation. Depending on the direction of the unit vector $\hat{d}$, the term inside the bracket in Eq. (3.18) gives different expressions. For example, if

$$\hat{d} = (1,0,0) \ ,$$

then

$$\sum_{\alpha} \delta[q-\alpha^{-1}\hat{d}\cdot(\vec{k}+\vec{K}_s)]$$

$$= 8[\delta\{q-(k_x+K_s^x)\} + \delta\{q+(K_x+K_s^x\}$$

$$+ \delta\{q-(k_y+K_s^y)\} + \delta\{q+(k_y+K_s^y)\}$$

$$+ \delta\{q-(k_z+K_s^z\} + \delta\{q+(k_z+K_s^z)\}]$$

Similar expressions may be written for $\hat{d} = \dfrac{1}{\sqrt{3}}(1,1,1)$.

CHAPTER IV: RESULTS

The self-consistent eigenvalues and eigenfunctions are obtained at 819 independent points in 1/48th of the Brillouin Zone.   This corresponds a mesh of 24 divisions along the Γ-H direction.   The points chosen may be characterized by integer values (n_x, n_y, n_z) representing coordinates $(k_x, k_y, k_z) = \frac{2\pi}{24a} (n_x, n_y, n_z)$, such that $n_x \geq n_y \geq n_z \geq 0$, where a is the low temperature lattice constant, a=5.429 (a.u.).   Considering the shape of the Brillouin Zone, two restrictions are imposed on (n_x, n_y, n_z); the sum of three n's should not be larger than 36, and the sum of n_x and n_y should be less or equal to 24.   Figure I displays the Brillouin Zone for a b.c.c. lattice; it also serves to identify certain special points and directions of high symmetry in the Brillouin Zone.

A.   Band Properties

The calculated energy band structure is shown in Fig. III.   The bands show a hybridization between the narrow d band and the broad s-p band.   In Table III some characteristic energy differences at higher symmetry points are listed and they are compared with corresponding values obtained by other authors.   Strictly speaking, such a comparison may not be very meaningful, because the

51

other works use different kinds of potential (muffin-tin) as in Ref. (17) and Ref. (10). Again, the values of the exchange parameter α are different in all the cases except in Ref. (17) and Ref. (10), where $\alpha=1$. One of these calculations[17] is a self-consistent calculation where as the other[10] one is not. At each $\vec{k}$ in the Brillouin Zone there exists a set of 38 Bloch functions which describe the 38 lowest bands. They are expressed as

$$\psi_n(\vec{k},\vec{r}) = \frac{1}{\sqrt{N}} \sum_i \sum_\mu e^{i\vec{k}\cdot\vec{R}_\mu} a_{ni}(\vec{k}) u_i(\vec{r}-\vec{R}_\mu) \ .$$

Construction of the Bloch function $\psi_n(\vec{k},\vec{r})$ has been discussed in Chapter II. At $\vec{k}$ with special symmetry and given band index n, the coefficients $a_{ni}(\vec{k})$ were found to possess the required transformation property.[40]

The ordering of the energy levels at the N point differs in different calculations. Our order at this point is the same as in the work of Asano and Yamashita but the energy differences are not the same.

The density of states was calculated from the energy bands computed at 819 points in 1/48th of the Brillouin Zone using the Gilat-Raubenheimer method.[23] Contributions from the critical points were included in the density of states. The Fermi energy was determined by filling up

states till one obtained a total of 6 electrons. Figure IV shows a computer plot of the density of states. The number of states per Ryd-atom per spin is shown as a function of energy. In order to obtain the correct density of states for both spins, this result should be multiplied by 2. The density of states at the Fermi energy (E_F=0.05308) was estimated to be 9.6 states/(atom-Ryd). The electronic specific heat coefficient $\gamma=\pi^2/3\ N(\varepsilon_F)K^2$, where K is the Boltzman's constant, was found to be 1.66 mJ/mol $^\circ K^2$. Since this value pertains to a paramagnetic state, it can not be compared directly with the results of the low temperature measurements which are made on antiferromagnetic chromium. However, an experimental value[41] for this coefficient can be estimated by extrapolation from measurements of the specific heats of Cr-Mo and Cr-W alloys to be $\gamma=2.9\times10^{-3}$ mJ/mol $^\circ K^2$. Part of the discrepancy may be attributed to neglect of the electron-phonon interaction.

B. Optical Absorption

Studies of the optical properties of Chromium may furnish some experimental evidence concerning the band structure. Bos and Lynch have investigated the optical absorption in the energy range in which interband transitions would be expected to be important. They find

a broad absorption peak between 1 and 2 eV, with indica-
tion of a shoulder near 2 eV, and an additional peak near
3.4 eV. Lenham and Treherne[43] find sharper structure
with peaks at 1.3 and 2.0 eV. Since we have not made a
detailed calculation of optical matrix elements, we can
not specify the location of maxima in a precise way. It
seems probable, on the basis of band structure shown in
Fig. III, that large regions of k space are involved in
all the transitions. Specifically, one would expect a
broad region of strong absorption from 1.3 to 2.1 eV
with a maximum near 2.0 eV associated with $\Sigma_1-\Sigma_3$ transi-
tion. These bands are roughly parallel with a separation
close to 2.0 eV over a range of k. Higher energy
absorption associated with $\Delta_5-\Delta_1$, P_4-P_3, F_3-F_3 transitions
is likely. The latter transitions correspond to energies
close to the peak reported at 3.4 eV.

C. Fermi Surface

A detailed study of the Fermi surface of Chromium
was made. Cross sections of the Fermi surface in various
symmetry planes were obtained. The Fermi surface consists
of electron and hole octahedra around Γ and H, respectively,
an electron ball on the 100 axis, and an ellipsoidal hole
pocket around N. These results are qualitatively in
accord with Lomer model and the results of other

calculations. A detailed description of the Fermi

surface is given in Table V . Some cross sections are

shown in Figs. V and VI .

The electron and hole octahedra exhibit the nesting

property required by current theories of antiferro-

magnetic Chromium. The quantity 1-δ defined in Fig.

describes the nesting. This quantity ranges from 0.976

to 0.955 in the (100) plane and 0.974 to 0.963 in a

slightly displaced plane defined by the normal vector

$\frac{2\pi}{a}$ (0,0,1/24). The experimental[44] result for $\underset{\sim}{Q}$ is 0.963

close to the Neél temperature and 0.951 at low tempera-

tures. The higher theoretical value which is obtained on

the (100) axis probably does not specify the most likely

value of Q since the contribution of states at this

point to the magnetic susceptibility is suppressed by

symmetry considerations regarding the matrix elements.

A detailed numerical calculation of the magnetic

susceptibility are required to specify a precise pre-

dicted value for the wave vector of the (SDW).

Some direct information concerning the Fermi surface

of paramagnetic Chromium can be obtained from the measure-

ments of Muhlstein[45] and collaborators of the phonon

dispersion relations using a neutron diffraction technique.

These authors observed Kohn anomalies in the vibration

spectrum both below and above the Neél temperature. Values

are reported for the length of the vectors AC and ED in

Fig. (VI). Our results, in units of $\frac{2\pi}{a}$, are (with experimental values in parenthesis): AC, 0.98 (0.98); ED, 0.427 (0.425).

Experimental information also exists concerning the dimensions of the hole pocket at N. This comes from measurements of the de Haas-van Alphen effect in anti-ferromagnetic state reported by Graebner and Marcus.[15] These authors find that the pocket is ellipsoidal with dimensions of 0.173, 0.234, and 0.268 A^{o-1} along NH, NΓ, and NP directions respectively. Our results are 0.229, 0.371 and 0.375 respectively. The agreement is not good. However, it is not certain that the results should be the same since the size of the pocket could be modified by the establishment of antiferromagnetic order.

D. Charge Density

The calculated charge density can be related to experiment through the calculation of X-ray scattering form factors. The scattering form factor is given as

$$F_x(\vec{K}) = \int e^{i\vec{K}\cdot\vec{r}} \rho(\vec{r}) \, d^3r$$

The wave functions obtained from the self-consistent calculation were used to compute $F(\vec{K})$. This quantity has been measured by Diana and Mazzone. In Table VII

we tabulate the results from the present calculation, the experiment, and the calculation utilizing the HF wave functions for free atom. Theoretical results tend to be larger than the experimental ones; but stay below the results obtained from the free atom calculation.

Some evidence that the charge distribution departs from spherical symmetry is seen from the fact that $F_x(330) \neq F_x(411)$. The ratio of these two quantities has also been measured by Diana and Mazzone. The theoretical value for this asymmetry ratio is in good agreement with the experimental result.

E. Compton Profile

The Compton profile $J(q)$ was calculated in the (100) and (111) directions using the wavefunctions obtained from the self-consistent calculation. The agreement with the experiment is rather good, except for small values of q. For large values of q the theoretical curve falls slightly below the experimental curve. Figures VIII and IX show the experimental and theoretical Compton profiles. The values of $J(q)$ are tabulated in Tables VIII and IX. The band Compton profile (Figs. IX and XII) was calculated by separating the contribution of the atomic core from the total Compton profile. Some features found in the band Compton profile are due to the structure of the Fermi surface.

REFERENCES

1. Brandt, G. B., and Rayne, J. A., Phys. Rev. 132, 1945 (1963); Sparlin, D. M., and Marcus, J. A., Phys. Rev. 144, 484 (1966).

2. Wakoh, S., and Yamashita, J., J. Phys. Soc. Japan 21, 1712 (1966); Tawil, R. A., and Callaway, J., Phys. Rev. B7, 4242 (1973).

3. Wakoh, S., and Yamashita, J., J. Phys. Soc. Japan 19, 1342 (1964); Hodges, L., Ehrenreich, H., and Lang, N. D., Phys. Rev. 152, 505 (1966); Langlinais, J., and Callaway, J., Phys. Rev. B5, 124 (1972); Callaway, J., and Wang, C. S., Phys. Rev. B7, 1096 (1973).

4. Overhauser, A. W., Phys. Rev. Letts 4, 462 (1960).

5. Overhauser, A. W., Phys. Rev. 128, 1437 (1962).

6. Rajagopal, A. K., Phys. Rev. 142, 152 (1966).

7. Fedders, P. A., and Martin, P. C., Phys. Rev. 143, 245 (1966).

8. Hamann, D. R., and Overhauser, A. W., Phys. Rev. 143, 183 (1966).

9. Lomer, W. M., Proc. Phys. Soc. (London) 80, 489 (1962); Lomer, W. M., Proc. Phys. Soc. (London) 84, 327 (1964).

10. Gupta, R. P., and Sinha, Phys. Rev. B3, 2401 (1971).

11. Kimball, J. C., Phys. Rev. 183, 533 (1969); Shibatani, A., Motizuki, K., and Nagamiya, T., 177, 984 (1968).

12. Asdente, M., and Friedel, J., Phys. Rev. 124, 384 (1961); Asdente, M., Phys. Rev. 127, 1949 (1962).

13. Loucks, T. L., Phys. Rev. 139, A1893 (1965).

14. Matheiss, L. F., Phys. Rev. 139, A1893 (1965).

15. Graebner, J. E., and Marcus, J. A., Phys. Rev. 175, 659 (1968).

16. Switendick, A. C., J. Appl. Phys. 37, 1022 (1966).

17. Asano, S., and Yamashita, J., J. Phys. Soc. Japan 23, 714 (1967).

18. Yasni, M., Hayashi, E., and Shimizu, M., J. Phys. Soc. Japan 29, 1446 (1970).

19. Lafon, E., and Lin, C. C., Phys. Rev. 152, 5971 (1966).

20. Tawil, R. A., and Callaway, J., Phys. Rev. B7, 4242 (1973).

21. Callaway, J., and Wang, C. S., Phys. Rev. B7, 1096 (1973).

22. Callaway, J., and Fry, J. L., in "Computational Methods in Band Theory" edited by P. M. Marcus, J. F. Janak, and A. R. Williams (Plenum, New York, 1971), p. 571.

23. Gilat, G., and Raubenheimer, L. J., Phys. Rev. 144, 340 (1966).

24. Hubbard, J., Proc. Roy. Soc. A276, 238 (1963); 277, 237 (1964); 287, 401 (1964); 285, 542 (1965); 296, 82, 100 (1966); Proc. Phys. Soc. (London) 84, 455

(1964).

25. Gutzwiller, M. C., Phys. Rev. Lett. $\underline{10}$, 159 (1963); Phys. Rev. $\underline{134}$, A923 (1964); $\underline{137}$, A1726 (1965).

26. Raimes, S., Phil. Mag. $\underline{45}$, 727 (1954).

27. Slater, J. C., Phys. Rev. $\underline{81}$, 385 (1951).

28. Slater, J. C., Wilson, T. M., and Wood, J. H., Phys. Rev. $\underline{179}$, 28 (1969).

29. Gaspar, R., Acta. Phys. Hung. $\underline{3}$, 263 (1954); Kohn, W., and Sham, L. J., Phys. Rev. $\underline{140}$, A1133 (1965).

30. Rajagopal, A. K., and Callaway, J., Phys. Rev. B$\underline{7}$, 1912 (1973).

31. Wachter, A. J. H., J. Chem. Phys. $\underline{52}$, 1033 (1970).

32. Matheiss, L. F., Phys. Rev. $\underline{134A}$, 970 (1964).

33. Platzman, P. M., and Tzoar, N., Phys. Rev. $\underline{139}$, A410 (1965).

34. Eisenberger, P., and Platzman, P. M., Phys. Rev. A$\underline{2}$, 415 (1970).

35. Platzman, P. M., and Wolff, P. A., in Waves and Interactions in Solid State Plasma, Suppl. $\underline{13}$, Solid State Physics, edited by H. Eherenreich, F. Seitz, and D. Turnbull, (Academic Press, New York, 1970).

36. Currat, R., DeCicco, P. D., and Weiss, R. J., Phys. Rev. B$\underline{4}$, 4256 (1971).

37. Phillips, W. C., and Weiss, R. J., Phys. Rev. B$\underline{6}$, 4213 (1972).

38. Eisenberger, P., Lam, L., Platzman, P. M., and Schmidt, C. P., Phys. Rev. B6, 3671 (1972).

39. Lundqvist, B. I., and Lydén, C., Phys. Rev. B4, 3360 (1971).

40. Callaway, J., Energy Band Theory, (Academic Press, New York, 1964).

41. Heiniger, F., Bucher, E., and Muller, J., Phys. Letts. 19, 163 (1965).

42. Bos, L. W., and Lynch, D. W., Phys. Rev. B2, 4567 (1970).

43. Lenham, A. P., and Treherne, D. M., in Optical Properties and Electronic Structures of Metals and Alloys, edited by F. Abeles (North Holland, Amsterdam 1966), p. 196.

44. Koehler, W., Moon, R. M., Trego, A. L., and Mackintosh, A. R., Phys. Rev. 151, 405 (1966).

45. Shaw, W. M., and Muhlestein, L. D., Phys. Rev. B4, 969 (1971); Muhlestein, L. D., Gurmen, E., and Cunningham, R. M., in "Neutron Inelastic Scattering" (IAEA, Vienna, 1972) p. 53.

46. Freeman, A. J., and Watson, R. E., Acta. Crysta. 14, 231 (1961); Watson, R. E., and Freeman, A. J., Acta. Crysta. 14, 27 (1961).

48. Weiss, R. J., (unpublished).

49. Matheiss, L. F., Phys. Rev. 139A, 1893 (1965).

TABLE I

$\vec{K}$	$V_c(\vec{K})$	$\Delta V_c(\vec{K})$	$V_{ex}(\vec{K})$	$\Delta V_{ex}(\vec{K})$
000	−1.70601	0.24519	−1.30717	−0.09047
110	−0.81356	−0.09334	−0.21997	0.02281
200	−0.59788	−0.02931	−0.025089	0.0163
211	−0.47854	−0.00667	−0.037669	−0.00312
220	−0.39924	−0.00190	−0.05225	−0.01038
310	−0.34203	0.00221	−0.03946	−0.00753
222	−0.29873	0.00083	−0.01612	−0.00154
321	−0.26486	0.00037	0.00124	0.00290
400	−0.23771	−0.00110	0.00667	0.00432
411	−0.21552	−0.00034	0.00236	0.00327
330	−0.21552	0.00044	0.00236	0.00327
420	−0.19709	0.00001	−0.00626	−0.00108
332	−0.18157	0.00063	−0.01417	−0.00102
422	−0.16834	0.00033	−0.01842	−0.00233
510	−0.15694	−0.00035	−0.01834	−0.00261
431	−0.15694	0.00030	−0.01834	−0.00261
521	−0.13835	−0.00001	−0.00977	−0.00104
440	−0.13068	0.00022	−0.00476	0.00004
433	−0.12386	0.00034	−0.00112	0.00091
530	−0.12386	.00009	−0.00112	0.00091

TABLE II

The calculated $E(\vec{k})$ for paramagnetic chromium in Rydberg units.
The symbols following the energies are irreducible representation
labels defined by B.S.W.

$\Gamma(0,0,0)$	-0.47894 1	-0.02765 25'	-0.02765 25'	-0.02765 25'	0.13127 12	0.13127 12
$\Delta(\frac{1}{4},0,0)$	-0.38666 1	-0.02436 5	-0.02436 5	0.00833 2'	0.07532 2	0.15228 1
$\Delta(\frac{1}{2},0,0)$	-0.20565 1	-0.06191 2	0.01779 5	0.01779 5	0.09980 2'	0.22730 1
$\Delta(\frac{3}{4},0,0)$	-0.19587 1	-0.19149 2	0.13636 5	0.19765 2'	0.51261 1	
$H(1,0,0)$	-0.24178 12	-0.24178 12	0.23940 25'	0.23940 25'	0.23940 25'	
$\Lambda(\frac{1}{8},\frac{1}{8},\frac{1}{8})$	-0.40935 1	-0.04775 3	-0.04775 3	0.03581 1	0.12376 3	0.12376 3
$\Lambda(\frac{1}{4},\frac{1}{4},\frac{1}{4})$	-0.24699 1	-0.10205 3	-0.10206 3	0.12946 3	0.12947 3	0.21701 1
$\Lambda(\frac{3}{8},\frac{3}{8},\frac{3}{8})$	-0.13250 3	-0.13250 3	-0.10857 1	0.14576 3	0.14576 3	0.48061 1
$P(\frac{1}{2},\frac{1}{2},\frac{1}{2})$	-0.11457 4	-0.11457 4	-0.11457 4	0.15240 3	0.15240 3	
$\Sigma(\frac{1}{8},\frac{1}{8},0)$	-0.43163 1	-0.04462 2	-0.02950 1	0.00807 3	0.11657 1	0.13289 4
$\Sigma(\frac{1}{4},\frac{1}{4},0)$	-0.32035 1	-0.08457 2	-0.03274 1	0.10284 3	0.10776 1	0.13779 4
$\Sigma(\frac{3}{8},\frac{3}{8},0)$	-0.26020 1	-0.12282 2	0.05022 1	0.12487 1	0.14477 4	0.21479 3
$N(\frac{1}{2},\frac{1}{2},0)$	-0.26154 1	-0.13812 2	0.12738 1	0.14847 4	0.15993 1'	0.26868 3

Table II   cont'd

$F(\frac{7}{8}, \frac{1}{8}, \frac{1}{8})$	-0.20296 3	-0.20296 3	0.09465 1	0.21124 3	0.21124 3	
$F(\frac{3}{4}, \frac{1}{4}, \frac{1}{4})$	-0.12352 3	-0.12352 3	-0.10230 1	0.16449 3	0.16449 3	
$F(\frac{5}{8}, \frac{3}{8}, \frac{3}{8})$	-0.16809 1	-0.08857 3	-0.08857 3	0.14897 3	0.14897 3	
$G(\frac{7}{8}, \frac{1}{8}, 0)$	-0.21753 1	-0.21327 4	0.15655 3	0.17507 1	0.24363 2	0.70598 4
$G(\frac{3}{4}, \frac{1}{4}, 0)$	-0.18646 1	-0.13292 4	0.01215 3	0.08137 1	0.25391 2	0.53410 4
$G(\frac{5}{8}, \frac{3}{8}, 0)$	-0.22879 1	-0.09809 3	-0.00760 4	0.09651 1	0.26433 2	0.34060 4
$D(\frac{1}{2}, \frac{1}{2}, \frac{1}{8})$	-0.24275 1	-0.14032 4	0.08724 3	0.13114 1	0.14905 2	0.35970 3
$D(\frac{1}{2}, \frac{1}{2}, \frac{1}{4})$	-0.19397 1	-0.14284 4	-0.00162 3	0.14018 1	0.15044 2	0.50312 3
$D(\frac{1}{2}, \frac{1}{2}, \frac{3}{8})$	-0.13945 1	-0.13707 4	-0.07000 3	0.14897 1	0.15183 2	0.66139

TABLE III

All energy in Ryd units	Asano Yamashita $\alpha=1$, K.K.R.	Gupta Sinha APW, $\alpha=1$	Yasui, et al. OPW – tight binding $\alpha=.725$	Present Calculation $\alpha=2/3$, tight binding
$\Gamma_{12}-\Gamma_1$	.57849	.709	.569	.61021
$\Gamma_{12}-\Gamma'_{25}$	.13324	.145	.136	.15892
$\Gamma'_{25}-\Gamma_1$	.44525	.573	.424	.45129
$H'_{25}-H_{12}$	.48483	.523	.467	.48118
$H_{15}-\Gamma_1$		1.330	1.097	1.26439
$H'_{25}-\Gamma'_{25}$	.23410	.238	.298	.26750
$\Gamma_{12}-H_{12}$	.38397	.421	.314	.37305
P_3-P_4	.25051	.303	.227	.26697
N_2-N_1	.13265	.170	.109	.12342
N_3-N_1	.50248	.558	.498	.53022
N_4-N_1	.02006			.02109
N'_1-N_4	.05309			.01146
$N_3-N'_1$	.04983		.069	0.10875

TABLE IV

Author	Density of States at Fermi Energy	Coefficient of Electronic Specific Heat $mJ/(oK^2\ mole)$
Loucks (Ref. 13)	7.10	1.23
Asano & Yamashita (Ref. 17)	12.1	2.1
Gupta & Sinha (Ref. 10)	7.36	1.27
Yasui, et al. (Ref. 18)	6.55	1.13
Present Theory	9.6	1.66
Heiniger, et al. (Ref. 41) (experiment)	-	2.9

TABLE V

I	Large electron surface about Γ	Approximately octahedral. No intersection with surfaces II and III.
II	Large hole surface about H	Approximately octahedral and slightly larger than surface I. Touches surface IV at six points along Γ-H directions at a distance $0.41 \ (\frac{2\pi}{a})$ from H points.
III	Small hole surface about N	Ellipsoidal with near circular cross section in NP plane, and elliptical cross section in ΓHN plane. No intersections with any surfaces.
IV	Electron Ball	Almost spherical with greatest deviation from a sphere in Γ-H direction. Touches surface II, and intersects surface I. Together with surface I known as the electron "jack".

TABLE VI

Identification	Present Calculation	Experiment
AC (Fig. VI)	0.98 $(\frac{2\pi}{a})$	0.98 $(\frac{2\pi}{a})$ *
DE (Fig. VI)	0.427 $(\frac{2\pi}{a})$	0.425 $(\frac{2\pi}{a})$ *
NA (Fig. V)	0.371 $\overset{o}{A}^{-1}$	0.234 $\overset{o}{A}^{-1}$ **
NB (Fig. V)	0.229 $\overset{o}{A}^{-1}$	0.173 $\overset{o}{A}^{1}$ **
"Radius" of the spherical hole around N, along N-P (Fig. VI)	0.375 $\overset{o}{A}^{1}$	0.268 $\overset{o}{A}^{-1}$ **

* Ref. 45

* Ref. 15

TABLE VII

$\vec{K}$	Exp (Ref. 46) $F(\vec{K})$	HF Theory (Ref. 47)	Present Theory $F(\vec{K})$
1,1,0	15.74$\pm$0.2	16.78	16.27
2,0,0	13.06$\pm$0.17	13.62	13.31
2,1,1	11.37$\pm$0.15	11.63	11.60
2,2,0	10.10+0.14	10.30	10.33
3,3,0			7.510
4,1,1			7.448
3,3,0/4,1,1	1.013$\pm$0.007		1.008

TABLE VIII

$J_{100}(q)$ $(a.u)^{-1}$			$J_{111}(q)$ $(a.u)^{-1}$		
q(a.u)	Total Compton Profile	Band Compton Profile	q(a.u)	Total Compton Profile	Band Compton Profile
0.0	5.053	2.068	0.0	5.471	2.489
0.096	5.027	2.047	0.056	5.484	2.506
0.193	4.980	2.017	0.111	5.425	2.452
0.290	4.909	1.975	0.167	5.372	2.407
0.386	4.833	1.939	0.223	5.236	2.283
0.483	4.701	1.861	0.279	5.108	2.171
0.579	4.537	1.763	0.334	4.952	2.036
0.676	4.383	1.686	0.390	4.788	1.896
0.772	4.197	1.588	0.446	4.674	1.811
0.869	3.976	1.465	0.502	4.522	1.692
0.965	3.757	1.351	0.557	4.430	1.637
1.062	3.528	1.234	0.613	4.295	1.545
1.158	3.247	1.074	0.669	4.217	1.514
1.255	2.997	0.939	0.725	4.099	1.444
1.352	2.737	0.799	0.780	4.018	1.416
1.545	2.380	0.672	0.892	3.845	1.355
1.738	1.967	0.470	1.003	3.627	1.250
1.931	1.683	0.372	1.115	3.333	1.095
2.124	1.483	0.334	1.226	2.968	0.865
2.317	1.328	0.320	1.338	2.663	0.700
2.703	1.042	0.241	1.561	2.354	0.666

TABLE VIII (cont'd)

$J_{100}(q)$ (a.u)$^{-1}$			$J_{111}(q)$ (a.u)$^{-1}$		
q(a.u)	Total Compton Profile	Band Compton Profile	q(a.u)	Total Compton Profile	Band Compton Profile
3.089	0.797	0.134	1.784	1.952	0.512
3.475	0.679	0.112	2.007	1.609	0.375
3.958	0.552	0.071	2.285	1.320	0.287
4.441	0.460	0.044	2.564	1.086	0.213
5.020	0.381	0.030	2.898	0.935	0.208
5.599	0.310	0.018	2.233	0.749	0.129
6.372	0.148	0.008	3.679	0.528	0.087
7.723	0.061	0.003	4.459	0.386	0.046
9.075	0.002	0.000	5.239	0.271	0.024

TABLE IX

q(a.u)	Experiment Ref. 48	Calculated HF Ref. 48	Experiment Ref. 48	Calculated HF Ref. 48
0	5.70+.15	5.03	5.31+.15	4.82
0.2	5.65	4.88	5.31	4.80
0.4	5.41	4.60	5.16	4.64
0.6	5.02	4.17	4.88	4.27
0.8	4.27	3.72	4.29	3.80
1.0	3.35+.15	3.46	3.70+.15	3.52
1.2	2.87	3.13	3.09	3.17
1.4	2.50	2.79	2.66	2.82
1.6	2.18	2.46	2.20	2.47
1.8	1.80	2.14	1.80	2.15
2	1.54+.15	1.86	1.55+.15	1.85
3	.78	.96	.80	.95
4	.58	.61	.58	.60
5	.43	.43	.43	.43

Figure 1

Figure 2

Figure 3

PARAMAGNETIC CHROMIUM

Figure 4

76
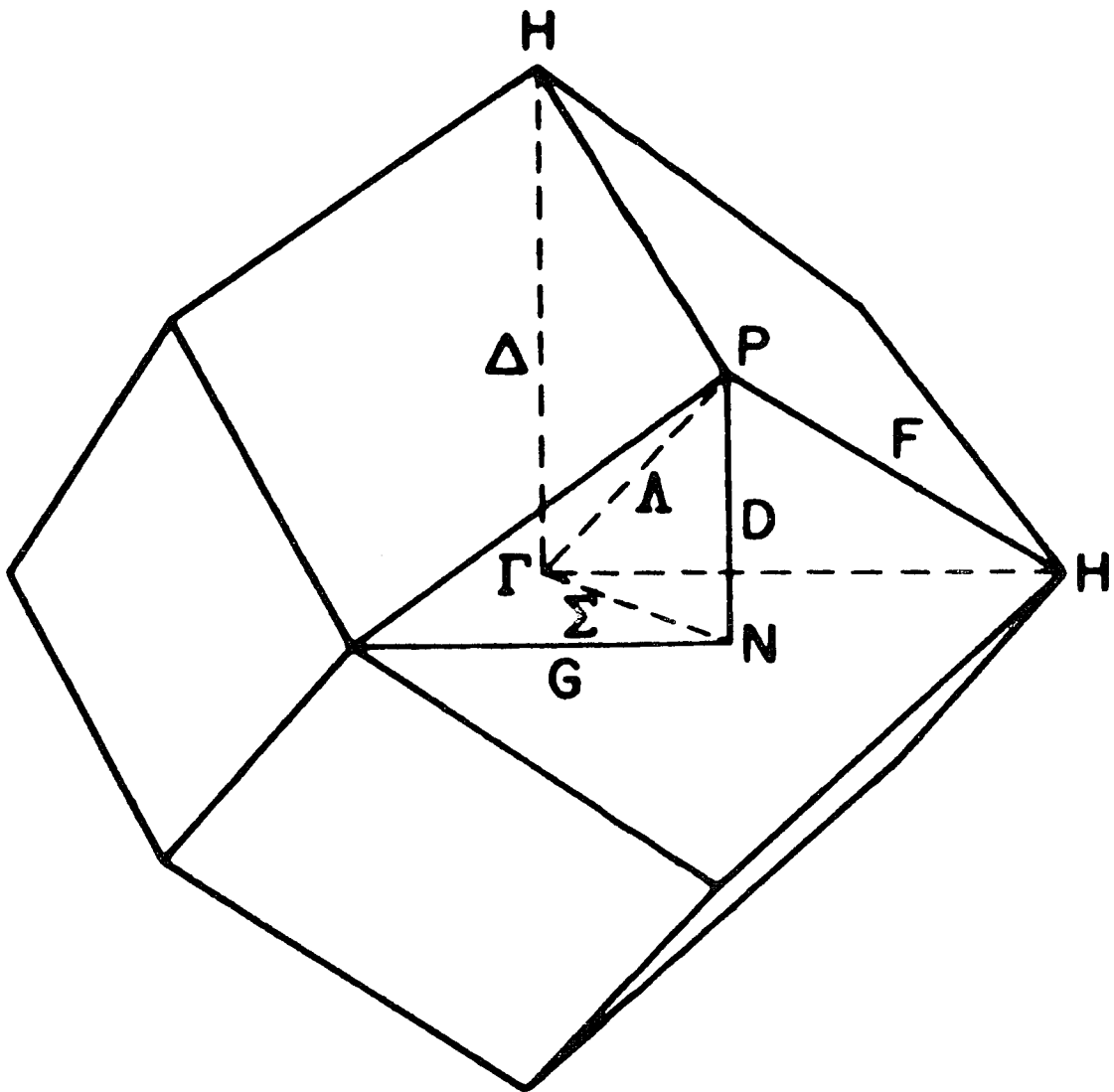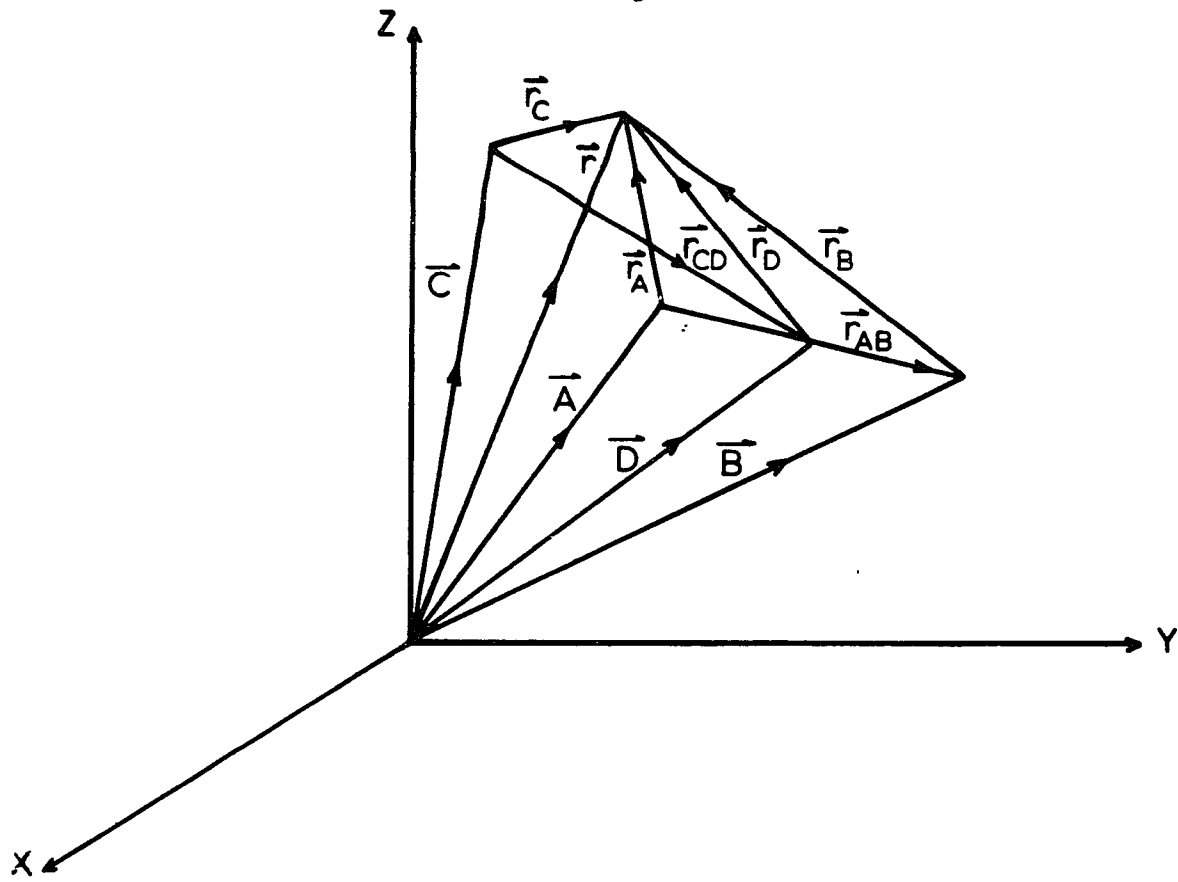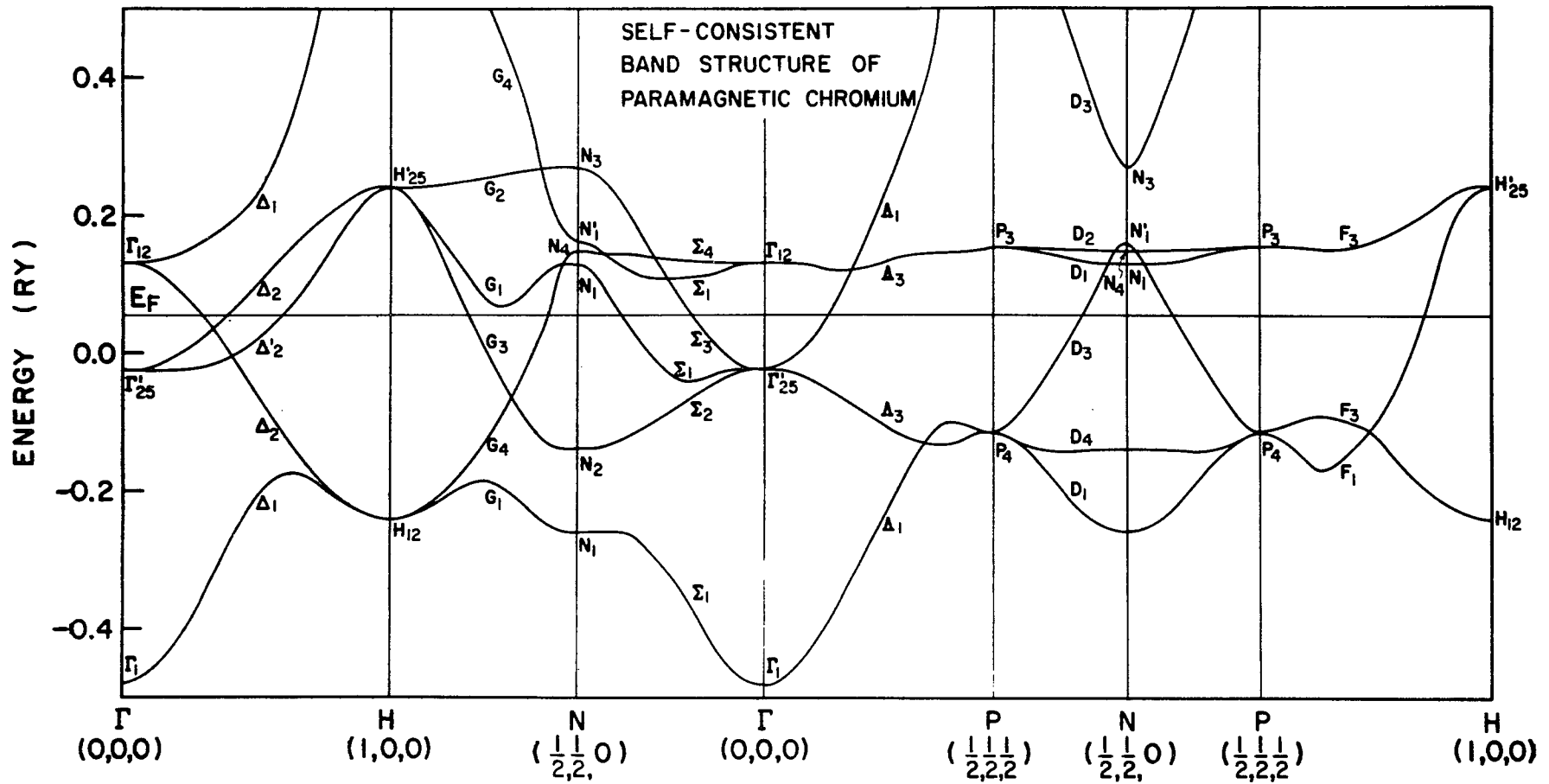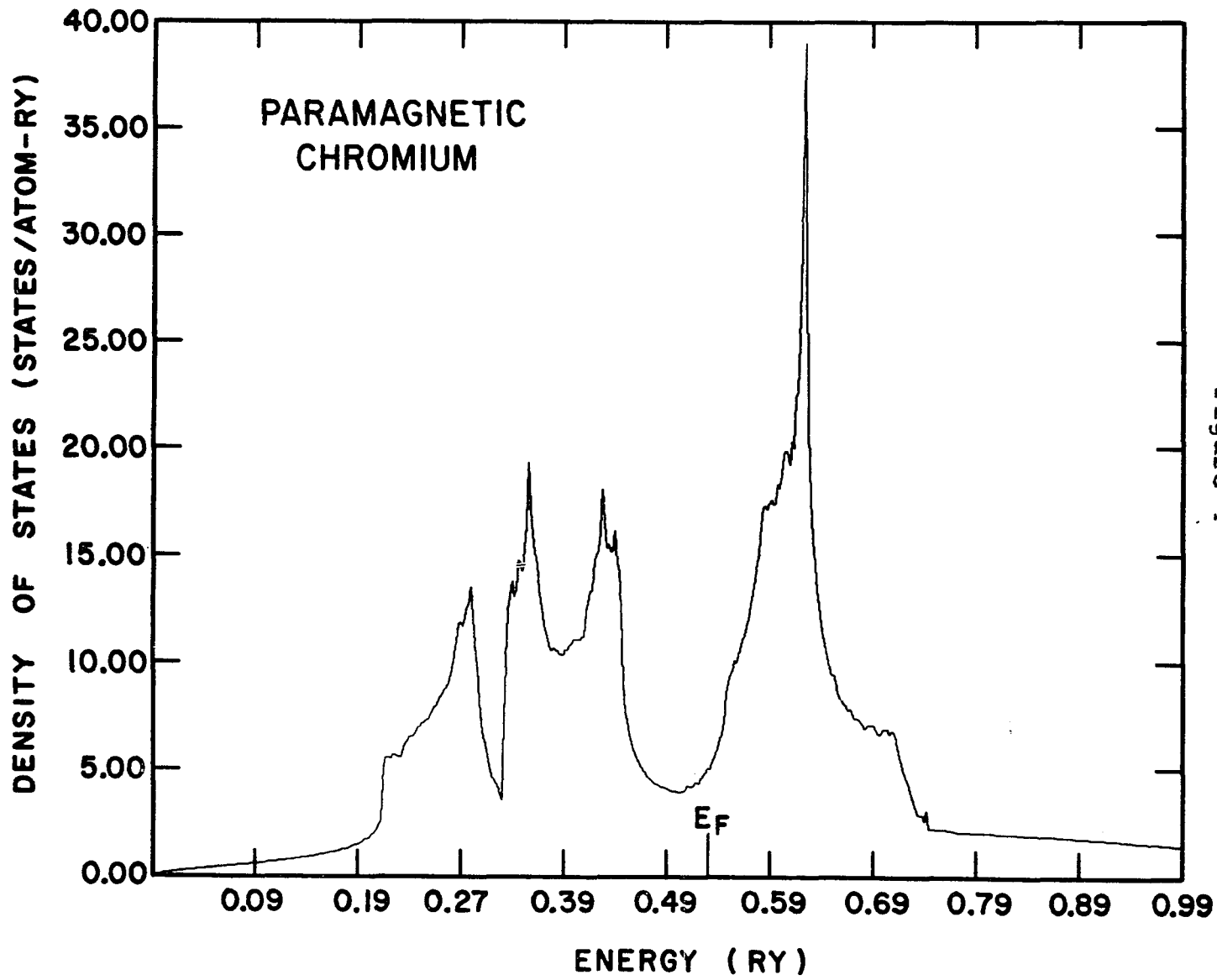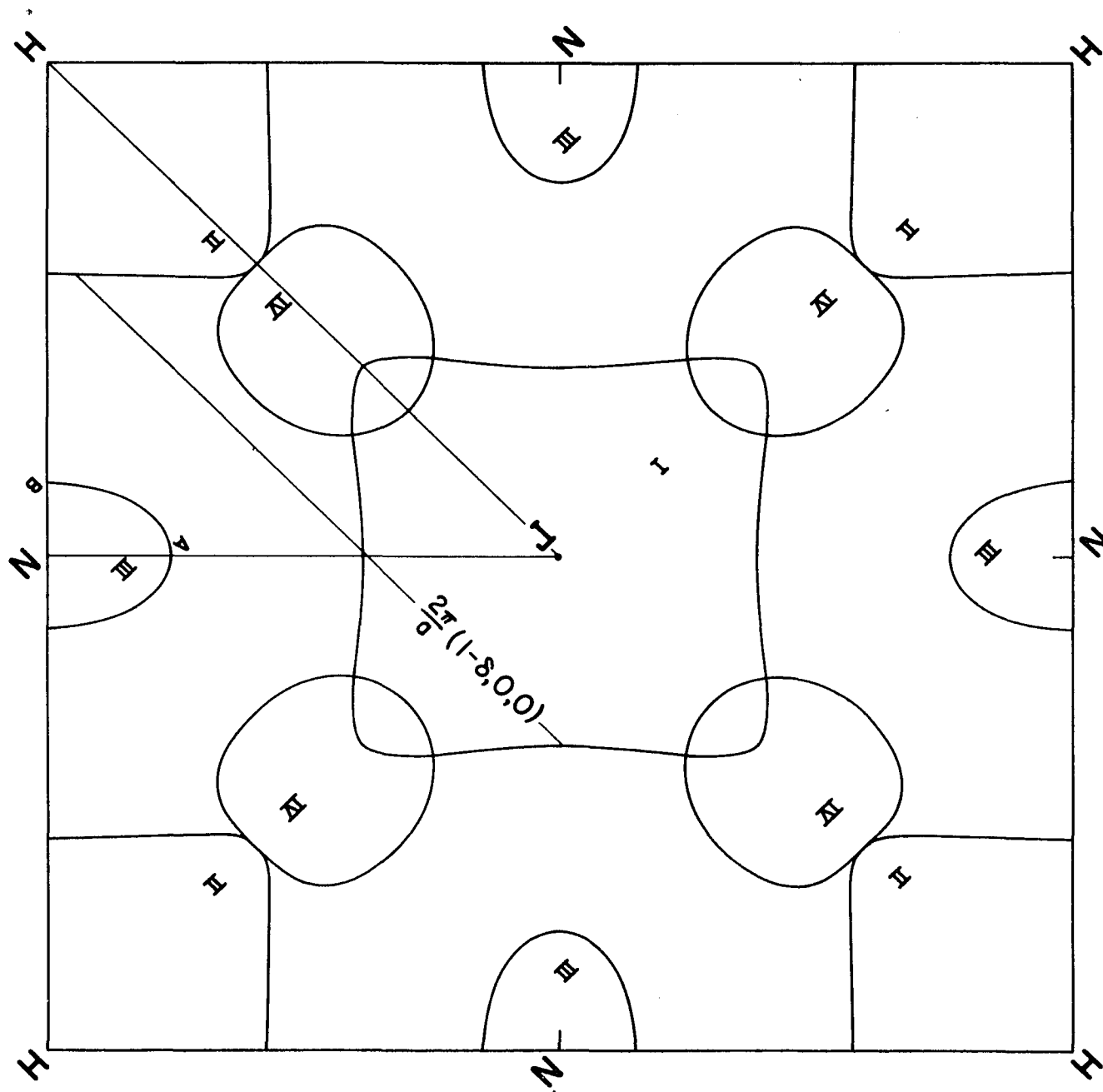
Figure 5
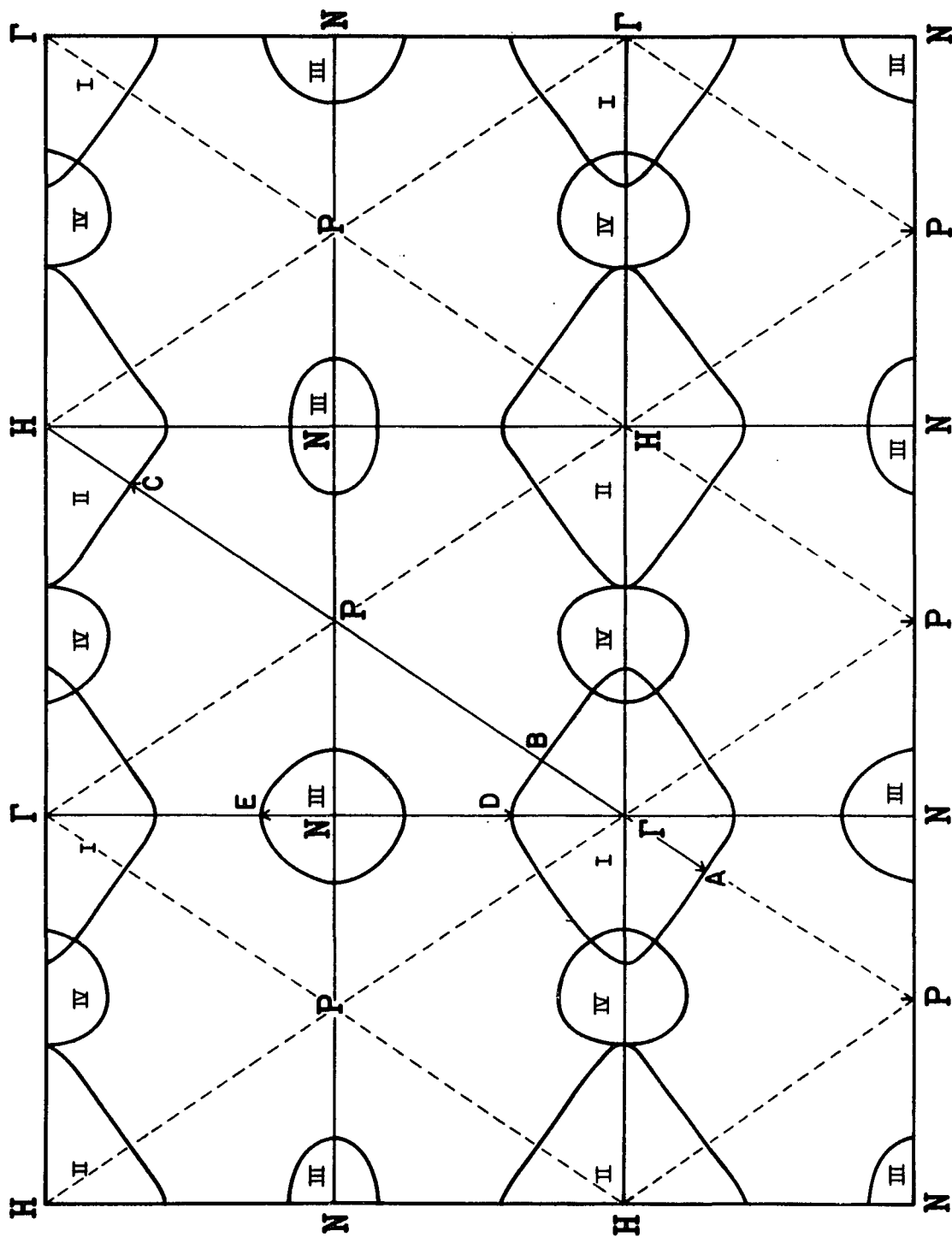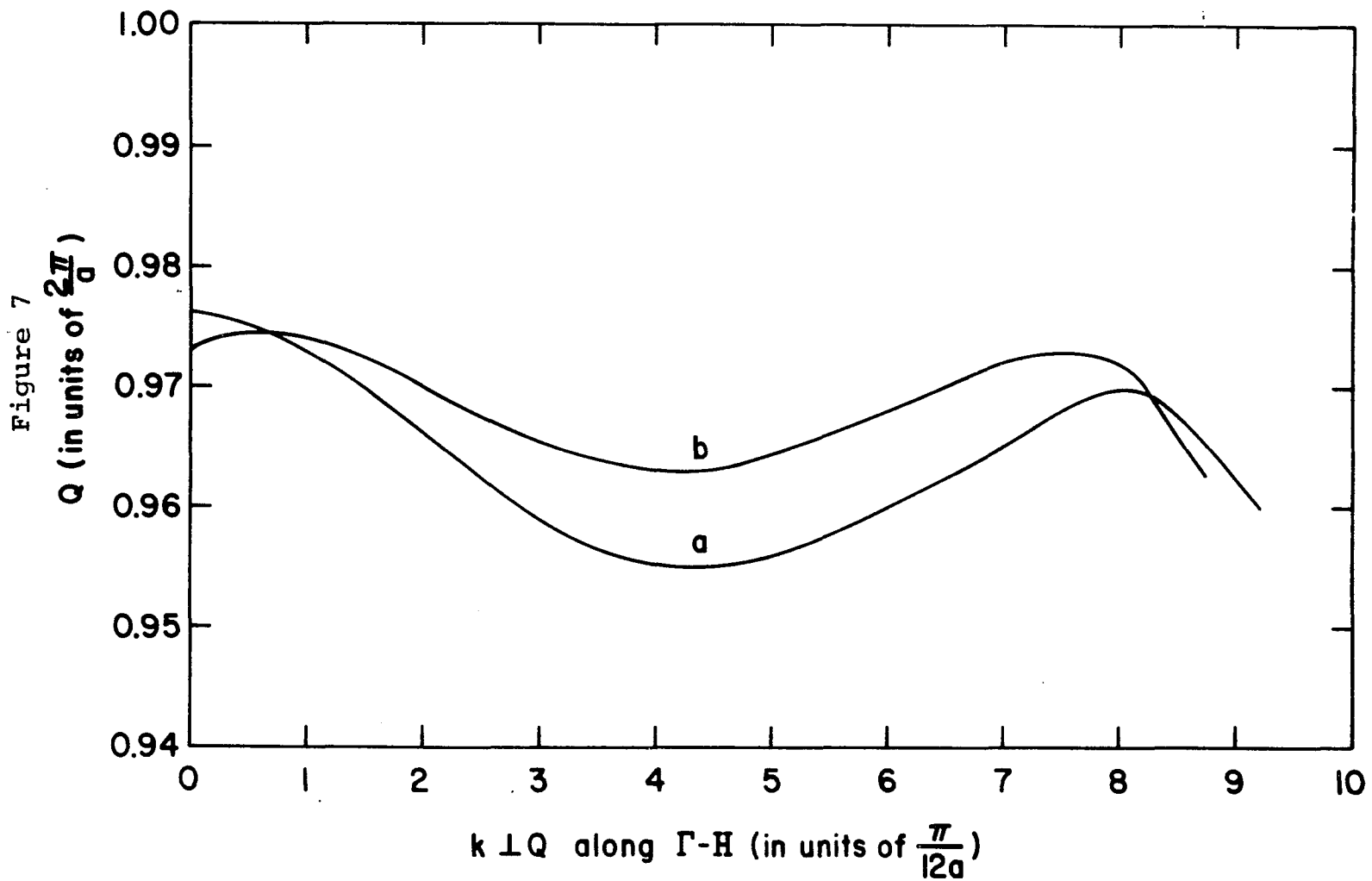
Figure 6
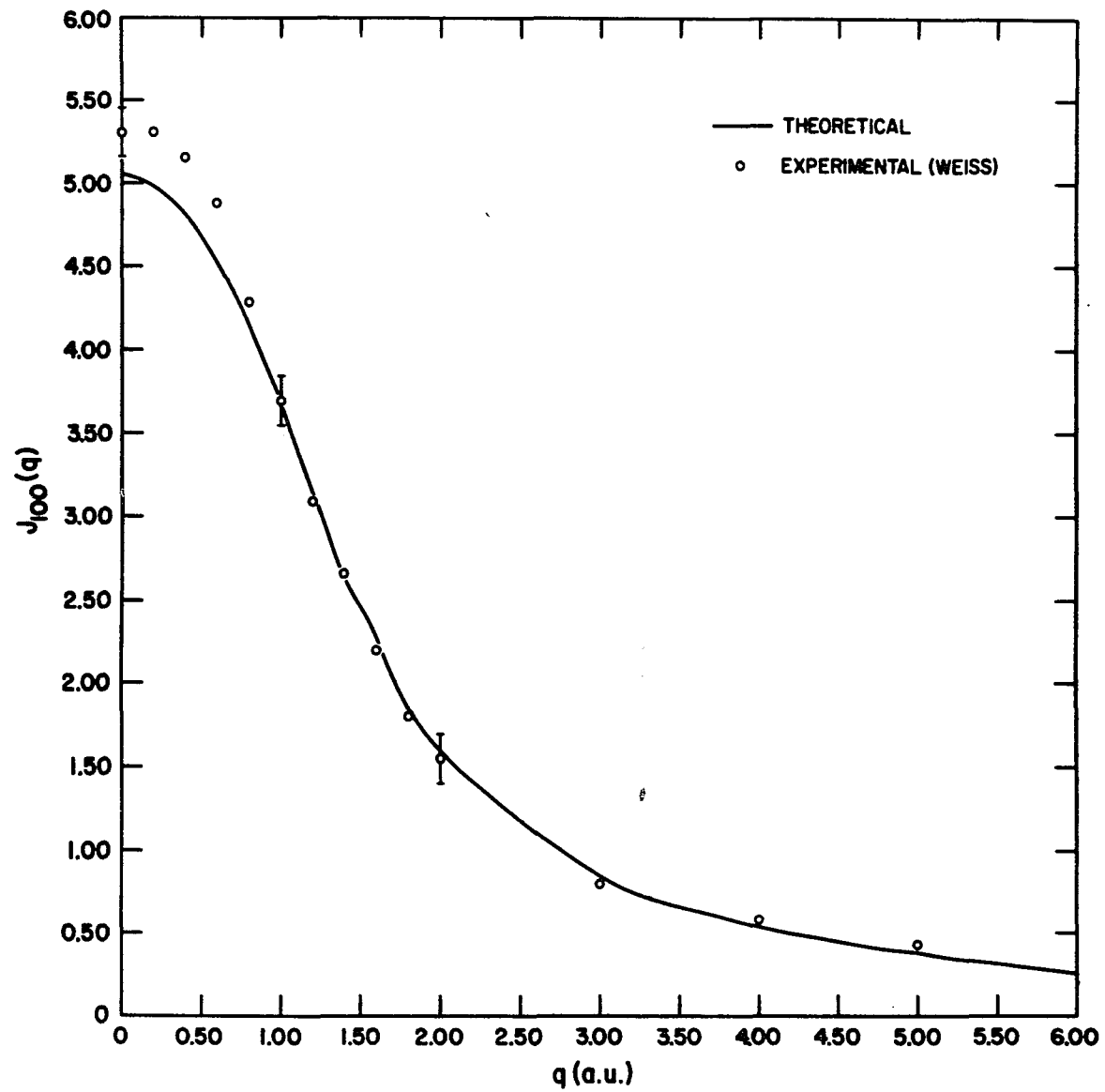
Figure 7
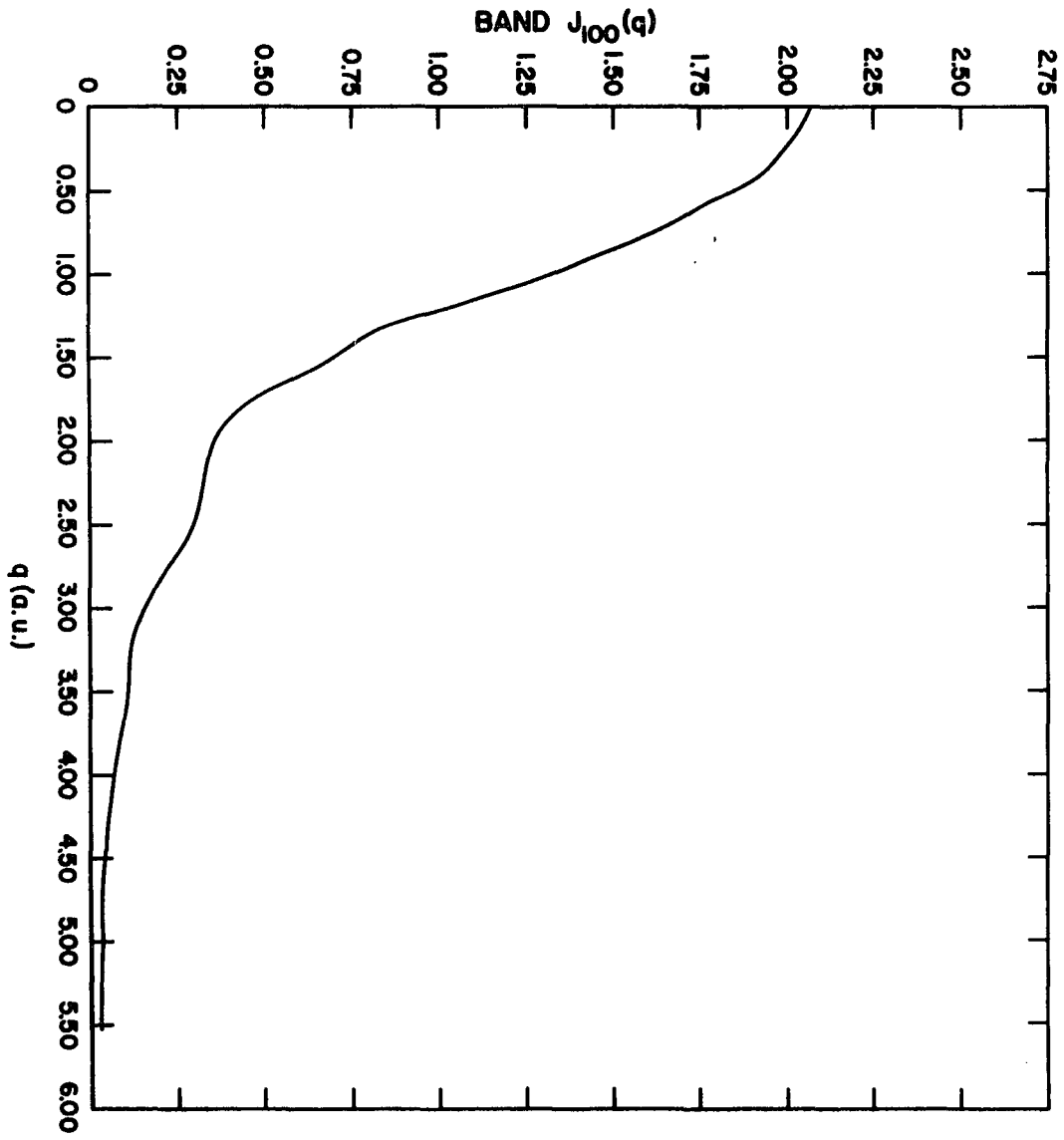
Figure 8

Figure 9

Figure 10
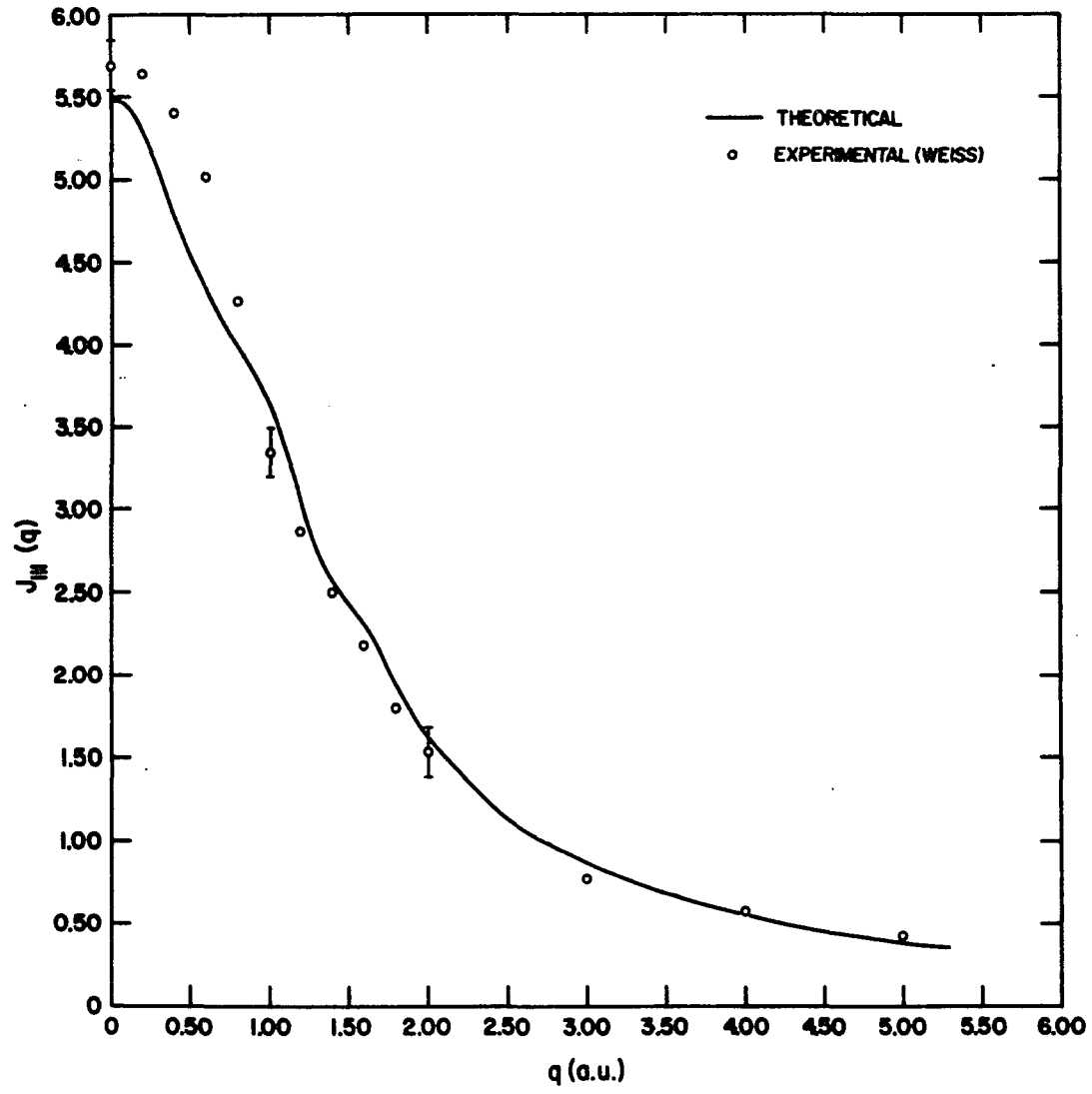
Figure 11
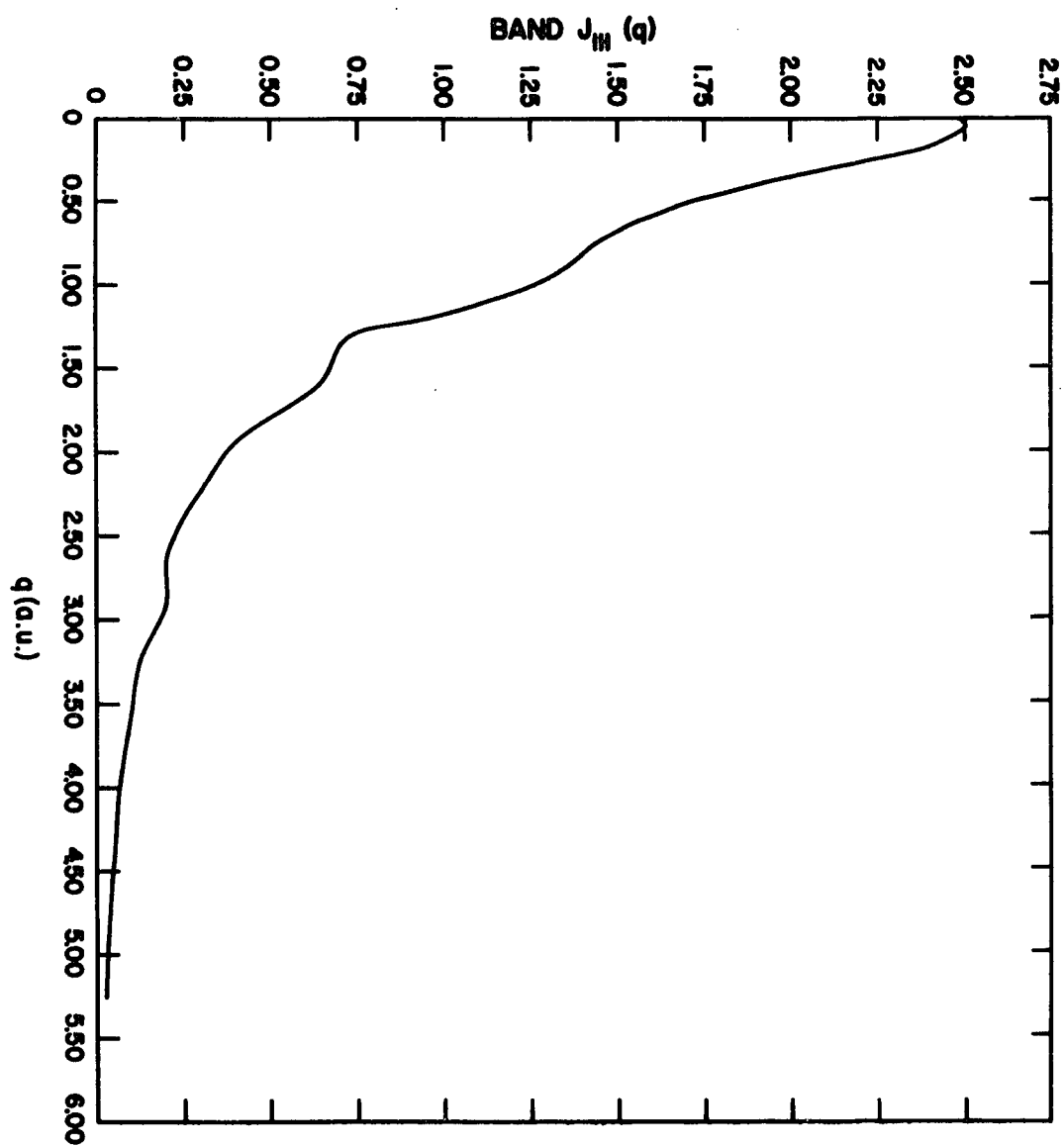
APPENDIX A

Below are the integral expressions used in the computation of the expectation value of 1 for the overlap, $-1/2\nabla^2$ for the kinetic energy, and $\cos(K_v \cdot r_{CD})$, where the wavefunctions are linear combinations of Gaussian-type orbitals, that is, $\exp(-a_1 r^2)$. Only the independent expressions are given. The others can be obtained by cyclic permutations of x, y, and z. We make use of the notation

$$\langle s|s \rangle = \langle G^S(a_1, \underline{r}-\underline{A}) | G^S(a_2, \underline{r}-\underline{B}) \rangle,$$

and using the definitions

$$\frac{d}{dA_x} \cos(K_v \cdot r_{CD}) = -K_x u \sin(K_v \cdot r_{CD})$$

$$\frac{d}{dB_x} \cos(K_v \cdot r_{CD}) = -K_x (1-u) \sin(K_v \cdot r_{CD})$$

$$\frac{d}{dA_x} \exp(-LR^2) = 2LX$$

$$\frac{d}{dB_x} \exp(-LR^2) = -2LR$$

we can derive the expressions. The symbols used are defined as

$$u = \frac{a_1}{a_1+a_2}$$

$$E = \exp\left(\frac{-K_y^2}{4(a_1+a_2)}\right)$$

$$L = \frac{a_1 a_2}{a_1+a_2}$$

$$W = \frac{1}{a_1+a_2}$$

$$D = \left[\frac{\pi}{a_1+a_2}\right]^{3/2}$$

$$T = \exp(-LR^2)$$

$$X = B_x - A_x$$

$$Y = B_y - A_y$$

$$Z = B_z - A_z$$

$$R^2 = X^2 + Y^2 + Z^2$$

$$\cos = \cos(K_v \cdot r_{CD})$$

$$\sin = \sin(K_v \cdot r_{CD})$$

$$K_x = K_{vx}$$

The constants below are the numerical factors involved in the spherical harmonics associated with the electron state wavefunctions.

$C_1 = 0.07957747$ $C_2 = 0.13783228$

$C_3 = 0.23873262$ $C_6 = 0.08897035$

$C_5 = 0.15410117$ $C_4 = 0.30820235$

$C_9 = 0.15410111$ $C_8 = 0.26691118$

$C_7 = 0.53382235$ $C_{15} = 0.09947184$

$C_{14} = 0.17229028$ $C_{13} = 0.34458056$

$C_{12} = 0.29841552$ $C_{11} = 0.59683104$

$C_{10} = 1.19366207$

We can derive all subsequent integrals from $\langle s|0|s\rangle$, where 0 is one of the operators, $-1/2\nabla^2$ or $\cos K_v \cdot r_{CD}$. Some are shown as follows:

$$\langle P_x|0|s\rangle = \frac{1}{2a_1}\frac{d}{dA_x}\langle s|0|s\rangle$$

$$\langle P_x|0|P_x\rangle = \frac{1}{2a_2}\frac{d}{dB_x}\langle P_x|0|s\rangle = \frac{1}{2a_1}\frac{d}{dA_x}\frac{1}{2a_2}\frac{d}{dB_x}\langle s|0|s\rangle$$

$$\langle d_{xy}|0|s\rangle = \frac{1}{2a_1}\frac{d}{dA_y}\langle P_x|0|s\rangle = \frac{1}{2a_1}\frac{d}{dA_y}\frac{1}{2a_2}\frac{d}{dA_x}\langle s|0|s\rangle$$

$$\langle d_{(x^2-y^2)}|0|s\rangle = \frac{1}{2a_1}\frac{d}{dA_x}\langle P_x|0|s\rangle - \frac{1}{2a_1}\frac{d}{dA_y}\langle P_y|0|s\rangle$$

$$\langle d_{(3z^2-r^2)}|0|s\rangle = \langle d_{(2z^2-x^2-y^2)}|0|s\rangle$$

$$= \frac{1}{a_1}\frac{d}{dA_z}\langle P_z|0|s\rangle - \frac{1}{2a_1}\frac{d}{dA_x}\langle P_x|0|s\rangle$$

$$- \frac{1}{2a_1}\frac{d}{dA_y}\langle P_y|0|s\rangle$$

KINETIC ENERGY INTEGRALS

$$\langle s|-\nabla^2|s\rangle = 2C_1 DTL(3-2LR^2)$$

$$\langle P_x|-\nabla^2|s\rangle = 2C_2 DTLWa_2 X(5-2LR^2)$$

$$\langle P_x|-\nabla^2|P_x\rangle = 2C_3 DTLW(2.5-7LX^2-LR^2+2L^2X^2R^2)$$

$$\langle P_x|-\nabla^2|P_y\rangle = 2C_3 DTL^2WXY(2LR^2-7)$$

$$\langle d_{xy}|-\nabla^2|s\rangle = 2C_4 DTLW^2a_2^2(X^2-Y^2)(7-2LR^2)$$

$$\langle d_{(x^2-y^2)}|-\nabla^2|s\rangle = 2C_6 DTLW^2a_2^2(2Z^2-X^2-Y^2)(7-2LR^2)$$

$$\langle d_{(3z^2-r^2)}|-\nabla^2|s\rangle = 2C_7 DTLW^2a_1 Y(3.5-9LX^2-LR^2+2L^2X^2R^2)$$

$$\langle d_{xy}|-\nabla^2|P_x\rangle = 2C_7 DTW^2a_1 Y(3.5-9LX^2-LR^2+2L^2X^2R^2)$$

$$\langle d_{xy}|-\nabla^2|P_z\rangle = 2C_7 DTLW^3La_1 a_2^2 XYZ(2R^2-9)$$

$$\langle d_{(x^2-y^2)}|-\nabla^2|P_x\rangle = 2C_8 DTLW^2a_2 X(7-2LR^2$$
$$+ (Y^2-X^2)(9L-2L^2R^2))$$

$$\langle d_{(x^2-y^2)} | -\nabla^2 | P_y \rangle = 2C_8 DTLW^2 a_2 Y(-7+2LR^2$$

$$+ (Y^2-X^2)(9L-2L^2R^2)$$

$$\langle d_{(x^2-y^2)} | -\nabla^2 | P_z \rangle = 2C_8 DTLW^2 a_2 Z(Y^2-X^2)(9L-2L^2R^2)$$

$$\langle d_{(3_z^2-r^2)} | -\nabla^2 | P_x \rangle = 2C_9 DTLW^2 a_2 X(2LR^2-7$$

$$+ (X^2+Y^2-2Z^2)(9L-2L^2R^2))$$

$$\langle d_{(3_z^2-r^2)} | -\nabla^2 | P_z \rangle = 2C_9 DTLW^2 a_2 Z(2(7-2LR^2)$$

$$+ (X^2+Y^2-2Z^2)(9L-2L^2R^2)$$

$$\langle d_{xy} | -\nabla^2 | d_{xy} \rangle = 2C_{10} DTLW^2 ((3.5-9LY^2)(1-2LX^2)$$

$$+ (2L^2Y^2-L)(2X^2+R^2-2LX^2R^2))$$

$$\langle d_{yz} | -\nabla^2 | d_{xy} \rangle = 2C_{10} DTL^2 W^2 XZ(-4.5+11LY^2+LR^2-2L^2Y^2R^2)$$

$$\langle d_{yz} | -\nabla^2 | d_{yz} \rangle = 2C_{10} DTLW^2 ((3.5-9LY^2)(1-2LZ^2)$$

$$+ (2L^2Y^2-L)(2Z^2+R^2-2LZ^2R^2))$$

$$\langle d_{zx}|-\nabla^2|d_{xy}\rangle = 2C_{10}DTL^2W^2YZ(11LX^2-4.5+LR^2-2L^2X^2R^2)$$

$$\langle d_{zx}|-\nabla^2|d_{yz}\rangle = 2C_{10}DTL^2W^2XY(11LX^2-4.5+LR^2-2L^2Z^2R^2)$$

$$\langle d_{zx}|-\nabla^2|d_{zx}\rangle = 2C_{10}DTLW^2(3.5-9LZ^2)(1-2LX^2)$$

$$+ (2L^2Z^2-L)(2X^2+R^2-2LX^2R^2))$$

$$\langle d_{(x^2-y^2)}|-\nabla^2|d_{xy}\rangle = 2C_{11}DTL^3W^2XY(X^2-Y^2)(11-2LR^2)$$

$$\langle d_{(x^2-y^2)}|-\nabla^2|d_{yz}\rangle = 2C_{11}DTL^2W^2YZ(9-2LR^2)$$

$$+ (X^2-Y^2)(11L-2L^2R^2)$$

$$\langle d_{(x^2-y^2)}|-\nabla^2|d_{zx}\rangle = 2C_{11}DTL^2W^2XZ(-9+2LR^2$$

$$+ (X^2-Y^2)(11L-2L^2R^2))$$

$$\langle d_{(x^2-y^2)}|-\nabla^2|d_{(x^2-y^2)}\rangle = 2C_{12}DTLW^2(7$$

$$+ (X^4+Y^4)(11L^2-2L^3R)-2LR$$

$$+ (X^2+Y^2)(4L^2R-18L)$$

$$+ X^2Y^2(4L3R-22L^2))$$

$$\langle d_{(3_z^2-r^2)} | -\nabla^2 | d_{xy} \rangle = 2C_{13}DTL^2W^2XY(18-4LR^2$$

$$+ (X^2+Y^2-2Z^2)(2L^2R^2-11L))$$

$$\langle d_{(3_z^2-r^2)} | -\nabla^2 | d_{yz} \rangle = 2C_{13}DTL^2W^2YZ(-9+2LR^2$$

$$+ (X^2+Y^2)(2L^2R^2-11L))$$

$$\langle d_{(3_z^2-r^2)} | -\nabla^2 | d_{x2-y2} \rangle = 2C_{14}DTL^2W^2(X^2-Y^2)$$

$$((X^2+Y^2-2Z^2)(2L^2R^2-11)$$

$$- 2(9-2LR^2))$$

$$\langle d_{(3_z^2-r^2)} | -\nabla^2 | d_{(3_z^2-r^2)} \rangle = 2C_{15}DTLW^2(21-6LR^2$$

$$- 2(9L-2L^2R^2)(X^2+Y^2+4Z^2)$$

$$+ (X^2+Y^2-2Z^2)(11L^2-2L^3R^2))$$

$$\cos(K_v \cdot r_{CD}) \text{ INTEGRALS}$$

$$<s|\cos|s> = C_1 DTE \cos$$

$$<P_x|\cos|s> = C_2 DTEW(a_2 X\cos - 1/2 K_x \sin)$$

$$<P_x|\cos|P_x> = C_3 DTEW((1/2 - LX^2 - 1/4 WK_x^2)\cos + 1/2 XK_x(2u-1)\sin)$$

$$<P_x|\cos|P_y> = C_3 DTEW^2(1/2(a_1 K_x Y - a_2 K_y X)\sin$$
$$- (a_1 a_2 XY + 1/4 K_x K_y)\cos)$$

$$<d_{xy}|\cos|s> = C_4 DTEW^2((a_2^2 XY - 1/4 K_x K_y)\cos - 1/2 a_2(YK_x + XK_y)\sin)$$

$$<d_{(x^2-y^2)}|\cos|s> = C_5 DTEW^2((a_2^2(X^2 - Y^2) - 1/4(K_x^2 - K_y^2))\cos$$
$$- a_2(XK_x - YK_y)\sin$$

$$<d_{(3_z^2-r^2)}|\cos|s> = C_6 DTEW^2(\cos(a_2^2(2Z^2 - X^2 - Y^2)$$
$$- 1/4(2K_z^2 - K_x^2 - K_y^2)) - a_2(2ZK_z - XK_x - YK_y)\sin)$$

$$<d_{xy}|\cos|P_x> = C_7 DTEW^2(\cos(1/4 XK_x K_y(2u-1) + 1/2 a_2 Y$$
$$- 1/2 a_2 K_x^2 WY - a_2 LX^2 Y) - \sin(1/2 a_2 K_x XY(1-2u)$$
$$+ 1/4 K_y - 1/2 LX^2 K_y K_x^2 W/8))$$

$$\langle d_{xy}|\cos|P_z\rangle = C_7 DTEW^3 (\cos(-1/4a_2K_z(XK_y-YK_x)+a_1Z(1/4K_xK_y$$

$$- a_2^2XY))-1/2\sin(K_z(a_2^2XY-1/4K_xK_y)-a_1a_2Z$$

$$(XK_y+YK_x)))$$

$$\langle d_{(x^2-y^2)}|\cos|P_x\rangle = C_8 DTEW^3 (\cos(a_1X(1/4(K_x^2-K_y^2-a_2^2(X^2-Y^2)))$$

$$- 1/2a_2K_x(XK_x-YK_y)+a_2X/W)$$

$$- \sin(-a_1a_2Y(XK_x-YK_y)+1/2K_y(a_2^2(X^2-Y^2)$$

$$- 1/4(K_x^2-K_y^2)-1/W)))$$

$$\langle d_{(x^2-y^2)}|\cos|P_y\rangle = C_8 DTEW^3 (\cos(a_1Y(1/4(K_x^2-K_y^2)-a_2^2(X^2-Y^2))$$

$$- 1/2a_2K_y(XK_x-YK_y)-a_2Y/W)$$

$$- 1/4(K_x^2-K_y^2)-1/W)))$$

$$\langle d_{(x^2-y^2)}|\cos|P_z\rangle = C_8 DTEW^3 (\cos(a_1Z(1/4(K_x^2-K_y^2)$$

$$- a_2^2(X^2-Y^2))-1/2a_2K_z(XK_x-YK_y))$$

$$- \sin(1/2K_z(a_2^2(X^2-Y^2)-1/4(K_x^2-K_y^2))$$

$$- a_1a_2Z(XK_x-YK_y)))$$

$$\langle d_{(3_z^2-r^2)}|\cos|P_x\rangle = C_9 DTEW^3 (\cos(1/4a_1 X(2K_z^2-K_x^2-K_y^2)$$

$$- a_2^2 a_1 X(2z^2-x^2-y^2)-1/2a_2 K_x$$

$$(2ZK_z-XK_x-YK_y)-a_2 X/W)$$

$$- \sin(-1/2K_x/W-K_x(2K_z^2-K_x^2-K_y^2)/8$$

$$+ 1/2K_x a_2^2(2z^2-x^2-y^2)$$

$$- a_1 a_2 X(2ZK_z-XK_x-YK_y)))$$

$$\langle d_{(3_z^2-r^2)}|\cos|P_z\rangle = C_9 DTEW^3 (1/4a_1 Z(2K_z^2-K_x^2-K_y^2)$$

$$- a_1 a_2^2 Z(2z^2-x^2-y^2)-1/2a_2 K_z(2ZK_z-XK_x-YK_y)$$

$$+ 2a_2 Z/W)-\sin(K_z/W+1/2a_2^2 K_z(2z^2-x^2-y^2)$$

$$- a_1 a_2 Z(2ZK_z-XK_x-YK_y)))$$

$$\langle d_{xy}|\cos|d_{xy}\rangle = C_{10} DTEW^3 (\cos(a_1 a_2 LX^2 Y^2+1/4L(Y^2 K_x^2+X^2 K_y^2)$$

$$- 1/2W(a_1-a_2)^2 XYK_x K_y-(K_x^2+K_y^2)/8$$

$$= 1/2a_1 a_2(X^2+Y^2)+K_x^2 K_y^2 W/16+1/4W)$$

$$+ \ 1/2(a_2-a_1)\sin((YK_x+XK_y)(LXY+1/4WK_xK_y)$$

$$- \ 1/2(XK_x+YK_y)))$$

$$\langle d_{zx}|\cos|d_{xy}\rangle = C_{10}DTEW^3(\cos(a_1a_2LX^2YZ+1/4L(K_x{}^2YZ+X^2K_yK_z)$$

$$+ \ 1/4(1-2u)XK_x(a_2ZK_y-a_1YK_z)-K_yK_z/8$$

$$- \ 1/2a_1a_2YZ+K_x{}^2K_yK_zW/16)$$

$$+ \ \sin(1/2L((a_2-a_1)XK_xYZ+a_2K_yX^2Z$$

$$- \ a_1X^2YK_z)+1/2(a_1YK_z-a_2ZK_y)(1/2-1/4WK_x{}^2)$$

$$+ \ W(a_2-a_1)XK_xK_yK_z/8))$$

$$\langle d_{xy}|\cos|d_{(x^2-y^2)}\rangle = C_{11}DTEW^3(\cos(a_1(X^2-Y^2)(a_2LXY$$

$$+ \ 1/2W(a_2-1/2a_1)K_xK_y)+W(K_x{}^2-K_y{}^2)$$

$$(K_xK_y/16+1/2a_2(a_1-1/2a_2)XY))+\sin((a_2LXY$$

$$- \ 1/2a_1WK_xK_y)(XK_x-YK_y)+(a_2W(K_x^2-K_y^2)/8$$

$$- 1/2a_1L(X^2-Y^2))(XK_y-YK_x)$$

$$+ 1/2(a_1+a_2)(XK_y-YK_x)))$$

$$<d_{zx}|\cos|d_{(c^2-y^2)}> = C_{11}DTEW^3(\cos(a_1a_2XZ(L(X^2-Y^2)-1)$$

$$- 1/2a_2^2WXZ(K_x^2-K_y^2)-1/4a_1^2WK_xK_z(X^2-Y^2)$$

$$+ 1/2L(XK_x-YK_y)(XK_z+ZK_x)$$

$$+ 1/4K_xK_z(1/4W(K_x^2-K_y^2)-1))$$

$$+ \sin((XK_z+ZK_x)(a_2W(K_x^2-K_y^2)/8$$

$$- 1/2a_1L(X^2-Y^2)+XK_x-YK_y)(a_2LXZ-1/4$$

$$a_1WK_xK_z)+1/2(a_1XK_z-a_2ZK_x)))$$

$$<d_{zx}|\cos|d_{(3_z^2-r^2)}> = C_{13}DTEW^3(\cos(-a_1a_2XZ-1/4K_xK_z$$

$$+ (2Z^2-X^2-Y^2)(a_1a_2XZL-1/4a_1^2WK_xK_z)$$

$$+ 1/4W(2K_z^2-K_x^2-K_y^2)(1/4K_xK_z-a_2^2XZ)$$

$$+ 1/2L(XK_z+ZK_x)(2ZK_z-XK_x-YK_y))$$

$$+ \sin(1/2 W a_2 (XK_z + ZK_x) (1/4 (2K_z^2 - K_x^2 - K_y^2)$$

$$- a_1^2 (2Z^2 - X^2 - Y^2)) - (a_2 + 1/2 a_1) XK_z$$

$$+ (a_1 + 1/2 a_2) ZK_x + (2ZK_z - XK_x - YK_y)$$

$$(a_2 LXZ - 1/4 W a_1 K_x K_z)))$$

$$\langle d_{(x^2-y^2)} | \cos | d_{(x^2-y^2)} \rangle = C_{12} DTEW^4 (\cos(a_1^2 a_2^2 (X^2 - Y^2)$$

$$- 1/2 (a_1^2 + a_2^2) (X^2 - Y^2) (K_x^2 - K_y^2)$$

$$+ a_1 a_2 (XK_x - YK_y)^2 - 2 a_1 a_2 (X^2 + Y^2) / W$$

$$+ (K_x^2 - K_y^2)^2 / 16 - 1/2 (K_x^2 + K_y^2) / W$$

$$- 1/W^2) + \sin((a_2 - a_1) (XK_x - YK_y)$$

$$(a_1 a_2 (X^2 - Y^2) + 1/4 (K_x^2 - K_y^2))$$

$$- (a_2 - a_1) (XK_x + YK_y)))$$

$$\langle d_{(x^2-y^2)} | \cos | d_{(3_z{}^2-r^2)} \rangle = C_{14} DTEW^3 (\cos(1/4W(1/4(K_x{}^2-K_y{}^2)$$

$$- a_2^2(X^2-Y^2)(2K_z{}^2-K_x{}^2-K_y{}^2)$$

$$+ W(2Z^2-X^2-Y^2)(a_1^2 a_2^2(X^2-Y^2$$

$$- 1/4a_1^2(K_x{}^2-K_y{}^2))$$

$$+ 2a_1 a_2(X^2-Y^2)+1/2(K_x{}^2-K_y{}^2)$$

$$+ L(2ZK_z-XK_x-YK_y)(XK_x-YK_y))$$

$$+ \sin(a_2 W(XK_x-YK_y)(1/4(2K_z{}^2-K_x{}^2$$

$$- K_y{}^2)a_1^2(2Z^2-X^2-Y^2))$$

$$+ (a_2 L(X^2-Y^2)-1/4a_1 W(K_x{}^2-K_y{}^2))$$

$$(2ZK_z-XK_x-YK_y)+(a_2-a_1)(XK_x-YK_y)))$$

$$\langle d_{(3_z{}^2-r^2)} | \cos | d_{(3_z{}^2-r^2)} \rangle = C_{15} DTEW^3 (\cos(a_1 a_2 L(2Z^2-X^2-Y^2)^2$$

$$- 2a_1 a_2(4Z^2+X^2+Y^2)+3/W$$

$$- 1/4W(a_1^2+a_2^2)(2Z^2-X^2-Y^2)$$

$$(2K_z{}^2 - K_x{}^2 - K_y{}^2)$$

$$+ \ L(2ZK_z - XK_x - YK_y)^2$$

$$+ \ W(2K_z{}^2 - K_y{}^2 - K_y{}^2)^2/16$$

$$- \ 1/2(4K_z{}^2 + K_x{}^2 + K_y{}^2))$$

$$+ \ (a_2 a_1)\sin((2ZK_z - XK_x - YK_y)$$

$$(L(2Z^2 - X^2 - Y^2) + 1/4W(2K_z^2 - K_x^2 - K_y^2))$$

$$- \ (4ZK_z + XK_x + YK_y)))$$

In the calculation of Compton profile one needs to calculate the Fourier transform of atomic functions. We list the Fourier transform of these functions for convenient reference.

The Fourier transform, $u_i(\vec{p})$, of an atomic function $u_i(\vec{r})$ was defined as

$$u_i(\vec{p}) = \frac{1}{\sqrt{\Omega}} \int e^{-i\vec{p}\cdot\vec{r}} u_i(\vec{r}) \, d^3r \, .$$

The atomic function $u_i(\vec{r})$ were expressed as linear combination of GTO (see Eq. (2.)). With the appropriate normalization constants the Fourier transforms of the atomic functions are given as follows:

S-functions

$$u_{ns}(\vec{p}) = \frac{1}{\sqrt{4\pi\Omega}} \sum_{i=1}^{14} c_{ni} \, N_s(\alpha_i) \, [\frac{\pi}{\alpha_i}]^{3/2} \, e^{-p^2/4\alpha_i}$$

P-functions

$$\begin{bmatrix} u_{nx}(\vec{p}) \\ u_{ny}(\vec{p}) \\ u_{nz}(\vec{p}) \end{bmatrix} = \frac{(-i)}{2} \cdot \sqrt{\frac{3}{4\pi\Omega}} \begin{bmatrix} p_x \\ p_y \\ p_z \end{bmatrix} \sum_{i=1}^{11} c_{ni} N_p(\alpha_i) \frac{\pi}{\alpha_i} [\frac{\pi}{\alpha_i}]^{3/2} e^{-p^2/4\alpha_i}$$

d-functions

$$
\begin{bmatrix} u_{xy}(p) \\ u_{yz}(p) \\ u_{zx}(p) \end{bmatrix} = -\frac{1}{4}\cdot\sqrt{\frac{15}{4\pi\Omega}} \begin{bmatrix} p_x p_y \\ p_y p_z \\ p_z p_x \end{bmatrix} N_d(\alpha_i)\ [\frac{\pi}{\alpha_i}]^{3/2}\ \frac{1}{\alpha_i^2}\ e^{-p^2/4\alpha_i}
$$

$$
u_{x^2-y^2}(\vec{p}) = -\frac{1}{4}\sqrt{\frac{15}{16\pi\Omega}}\,(p_x^2-p_y^2)N_d(\alpha_i)\ [\frac{\pi}{\alpha_i}]^{3/2}\ \frac{1}{\alpha_i^2}\ e^{-p^2/4\alpha_i}
$$

$$
u_{3z^2-r^2}(\vec{p}) = -\frac{1}{4}\cdot\sqrt{\frac{5}{16\pi\Omega}}\,(3p_z^2-p^2)N_d(\alpha_i)\ [\frac{\pi}{\alpha_i}]^{3/2}\ \frac{1}{\alpha_i^2}\ e^{-p^2/4\alpha_i}
$$

VITA

Jagannath Rath was born on September 27, 1946 in Orissa, India. He graduated from Ranihat High School in 1960. He received the degree of Master of Science in Physics from the University of Illinois, Chicago in July 1969. He entered Louisiana State University, Baton Rouge, in July 1970. He is now a candidate for the degree of Doctor of Philosophy in the Department of Physics and Astronomy.
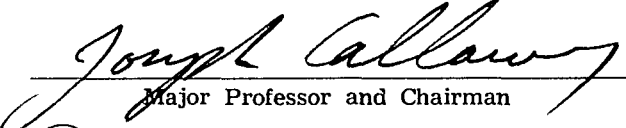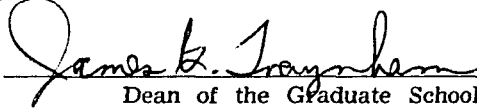
EXAMINATION AND THESIS REPORT
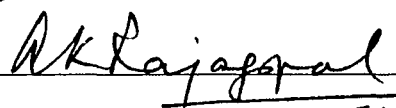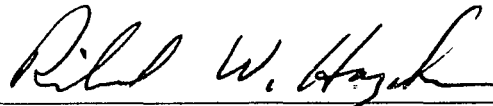
Candidate: Jagannath Rath

Major Field: Physics

Title of Thesis: Energy Bands in Paramagnetic Chromium

Approved:

Joseph Callaway
Major Professor and Chairman

James B. Traynham
Dean of the Graduate School

EXAMINING COMMITTEE:

William G. Lamb

John Kimball

A K Rajagopal

Richard W. Hayek

Date of Examination:

June 27, 1973